Investigating energy performance of large-scale seasonal storage in the district heating system of chifeng city

Measurements and model-based analysis of operation strategies

Xu, Luyi; Guo, Fang; Hoes, Pieter-Jan; Yang, Xudong; Hensen, Jan

DOI
10.1016/j.enbuild.2021.111113

Publication date
2021

Document Version
Final published version

Published in
Energy and Buildings

Citation (APA)
Xu, L., Guo, F., Hoes, P.-J., Yang, X., & Hensen, J. (2021). Investigating energy performance of large-scale seasonal storage in the district heating system of chifeng city: Measurements and model-based analysis of operation strategies. *Energy and Buildings*, *247*, Article 111113. https://doi.org/10.1016/j.enbuild.2021.111113

Energy & Buildings 247 (2021) 111113

Contents lists available at ScienceDirect

Energy & Buildings

journal homepage: www.elsevier.com/locate/enb

Investigating energy performance of large-scale seasonal storage in the district heating system of chifeng city: Measurements and model-based analysis of operation strategies

Luyi Xu [a,c,*], Fang Guo [b], Pieter-Jan Hoes [a], Xudong Yang [b,*], Jan L.M. Hensen [a]

[a] Department of the Built Environment, Eindhoven University of Technology, PO Box 513, 5600 MB Eindhoven, the Netherlands
[b] Department of Building Science and Technology, Tsinghua University, 100084 Beijing, China
[c] Faculty of Industrial Design Technology, Delft University of Technology, Postbus 5, 2600 AA Delft, the Netherlands

ARTICLE INFO

Article history:
Received 7 October 2020
Revised 8 May 2021
Accepted 11 May 2021
Available online 19 May 2021

Keywords:
Borehole thermal energy storage
Industrial waste heat
TRNSYS
Modelica
Model validation

ABSTRACT

This paper presents a modeling and simulation method that supports energy performance assessment and operation strategy investigation of borehole thermal energy storage in the Chifeng district heating (DH) system. A living laboratory in Chifeng, China that integrates a 0.5 million m^3 borehole thermal energy storage system, an on-site solar thermal plant and excess heat from a copper plant is presented. The research adopts Modelica models from open source libraries to evaluate the system. The validity of the borehole thermal energy storage model is evaluated through an inter-model comparison study and an empirical validation test. We used the validated model to investigate three operation strategies. We conclude that the time-scheduled combined operation strategy is more beneficial for the studied system regarding CO_2 emission reduction.

1. Introduction

The district heating system of Chifeng city in Inner Mongolia Province, China is experiencing a transition from coal-fired boilers to sustainable and renewable heat sources. A seasonal energy imbalance between heating supply and heating demand is common in district heating systems with sustainable and renewable heat sources. Hence, implementing seasonal thermal energy storage (STES) in such systems can be beneficial in reducing the imbalance. Since the overall efficiency of STES is greatly influenced by its operational strategy, this paper aims to investigate the operation strategy of a STES in an existing district heating system in Chifeng. Modeling and simulation is conducted for the investigation. The following subsections provide details and background information about the district heating system in Chifeng.

1.1. District heating system of Chifeng city

China is witnessing a rapid expansion of its building stock, resulting in ever increasing energy demands. Currently, space heating is responsible for the largest part of the energy use of households and offices. Therefore, the Chinese government has developed a national heating reform to improve building energy efficiency. As part of an effective approach to improving total energy efficiency, development of district heating systems has grown exponentially since 2005 [1]. In addition, the government has set a target of increasing the share of non-fossil energy of the total primary energy consumption to 20% by 2030 (The 13th Five Year Plan for the development of renewable energy). One of the key objectives is to use renewable energy sources (RES) to substitute 150 million metric tons of energy from fossil fuels in the heating and domestic sector [2]. Chifeng City in Inner Mongolia Province has been chosen by the government as one of pilot cities to boost RES use.

Chifeng City is one of the first cities to have installed a district heating system in China. A large part of the heat was supplied by small capacity, neighborhood coal-fired boilers. In recent years, many of these boilers were shut down due to their low efficiencies and their high (polluting) emissions. However, as a result of urbanization, the demand for district heating in Chifeng City has increased by two to three million m^2 heated area every year. In

* *Corresponding authors at: Department of the Built Environment, Eindhoven University of Technology, PO Box 513, 5600 MB Eindhoven, the Netherlands (L. Xu). Department of Building Science and Technology, Tsinghua University, 100084 Beijing, China (X. Yang)

E-mail addresses: l.xu2@tue.nl (L. Xu), xyang@tsinghua.edu.cn (X. Yang).

https://doi.org/10.1016/j.enbuild.2021.111113
0378-7788/

alignment with the national objectives, the local authority of Chifeng City planned to introduce more renewable energy sources in the district heating system. Therefore, it was essential for the city to evaluate alternative (sustainable) heat sources.

Since 2013, one of the new heat sources of the district heating system is a copper plant located in the south of Chifeng City. The plant produces a significant amount of waste heat as a result of its industrial processes; the excess heat has a peak power of 20 MW_{th}. This excess heat is serving a residential area (of 11 thousand residents) and the office buildings of the copper plant. Although the amount of the excess heat is significant, the increased needs at both the demand side and the supply side promote the exploration of utilizing industrial waste heat to its fully extend.

1.2. District heating and seasonal thermal energy storage

District heating (DH) is one part of urban energy infrastructures. It connects buildings in a neighborhood, town, city or even countrywide through a network of pipes to provide space heating and domestic hot water. District heating was first introduced in United States in the 1880 s, and a few decades later it was commercially implemented in Europe. Since then, four generations of DH have been developed. The fourth generation in this line of development of district heating systems (4GDH), as defined in [3], are generally highly energy efficient and able to exploit energy diversity in heating generation. 4GDH systems provide flexibility on the utilization of renewable energy sources (RES) and low-grade supply sources, such as heat recycled from chillers or industrial surplus. The district heating system of Chifeng undergoes a generation transition to fully exploit the potentials of 4GDH.

The district heating system of Chifeng only operates during the heating season (from 16th of October to 15th of April). Since there is no heating demand during the non-heating season (16th of April to 15th of October), a considerable amount of heat of the copper plant is released into the environment, therefore the full potential of the waste heat is not used. To deal with this mismatch between supply and demand, it would be beneficial to include seasonal thermal energy storage in the district heating system [4–8]. Studies have shown that implementing STES can reduce overall system costs [9–12]. STES systems can be charged during the summer, for instance by solar thermal production or industrial waste heat, and retain the energy for later use during the colder winter months [13–15]. STES seems a promising technology to exploit the full potential of the waste heat from the copper plant. Therefore, initiated by the collaboration between Tsinghua University and Chifeng Heran Energy-saving Science and Technology Co. Ltd., a concept of a living laboratory is proposed to investigate the feasibility of implementing STES in the district heating system in Chifeng [16]. In the living laboratory, a collaboration network is formed among universities, the local thermal network provider and operator, and product providers (e.g. solar thermal collector). The living lab performs as (1) an experimental platform to test design options and operational strategies, (2) a sustainable energy heating plant as an actual operated application in a district heating network, and (3) a data source for field-scale long-term monitoring of a large-scale BTES [16].

1.3. A living laboratory for district heating and borehole thermal energy storage (BTES)

Due to the fact that STES normally has great volume, STES is mostly buried under the ground [5]. The typical forms of underground STES are borehole thermal energy storage (BTES), aquifer thermal energy storage (ATES) and cavern thermal energy storage (CTES). The last form of underground STES is technically feasible but not commercialized due to high investment costs [17,18]. In this regard, ATES and BTES are the most promising technologies [19,20]. Although ATES systems have shorter payback times than BTES systems, it is not always possible to realize an ATES system due to geological conditions. In the case of Chifeng City, a viability study showed that the soil is not favorable for an ATES system. Therefore, BTES was the chosen STES technology for the living laboratory. Fig. 1 shows one of the configurations of the living laboratory in the non-heating season and in the heating season. The system of the living laboratory consists of a circulation loop and three main subsystems. The subsystems are an industrial waste heat recovery system, a solar thermal system and a borehole thermal energy storage system. Each subsystem is connected to the circulation loop via a heat exchanger. The excess heat from the copper plant, with a yearly heating capacity of 32.4 GWh, serves as the main heating supply source. The modularized solar thermal subsystem, consisting 336 solar thermal collectors, represents another heat source. The solar thermal subsystem is used to boost the water temperature in the system circulation loop. The solar thermal subsystem contributes in injecting more heat in *non-heating season* and delivering warmer water to the DH network in the *heating season*. The solar thermal subsystem is designed to contribute 0.42 GWh on annual heating production. The main design parameters of the system are listed in Appendix A. According to the project plan, six modules of the solar thermal collector arrays will be installed in the living lab. As in the initial phase of the project, only one module (336 collectors) was constructed and included in the following analysis in this paper. A detailed description of the system and the evaluation of the design options can be found in previous studies [16,46].

In the *non-heating season*, the BTES is charged by industrial waste heat and solar thermal sources. The heat carrier fluid returns to the industrial waste heat subsystem (IWH1) after charging the BTES. The IWH source (IWH1) is waste heat from slag flashing water during the industrial processes with an average temperature of 70 °C (fluctuating from 40 °C to 90 °C). It provides the majority of heat injected into the BTES. Since the temperature level of the IWH source is not very high, it is then more practical to heat the heat carrier by the IWH subsystem first then by the STES subsystem than the other way around, though the current configuration may result in a relatively low output efficiency of the STES subsystem. To cope with this issue, an investigation of different operation mode with the combination of different IWH sources (with higher temperature level) will be performed as future work. The flexible design of the living lab makes it possible for system operators and researchers to test different operation modes [16].

In the *heating season*, the heat carrier fluid runs in a reverse direction. The return heat carrier fluid (around 45 °C) from the heating demand side flows through the BTES to extract heat. The solar thermal subsystem (STS) with a modularization design is adopted to further increases the temperature of the heat carrier fluid. The heat carrier fluid then serves as heating supply to the heating demand side. Therefore, the heating supply temperature at the heating demand side highly depends on the outlet temperature of the BTES subsystem. Another IWH source (IWH2) is connected to the pilot system as a back-up heat source. The designed heating supply temperature at the heating demand side is 55 °C. The back-up heat source (IWH2) is activated when the heating supply temperature cannot meet the required design value.

1.4. BTES operation strategies

The main goal of the system is to increase the use of RES and to reduce CO_2 emissions in the district heating sector. An additional goal of the pilot system is to reduce the usage of the back-up IWH subsystem (IWH2) in the heating season as much

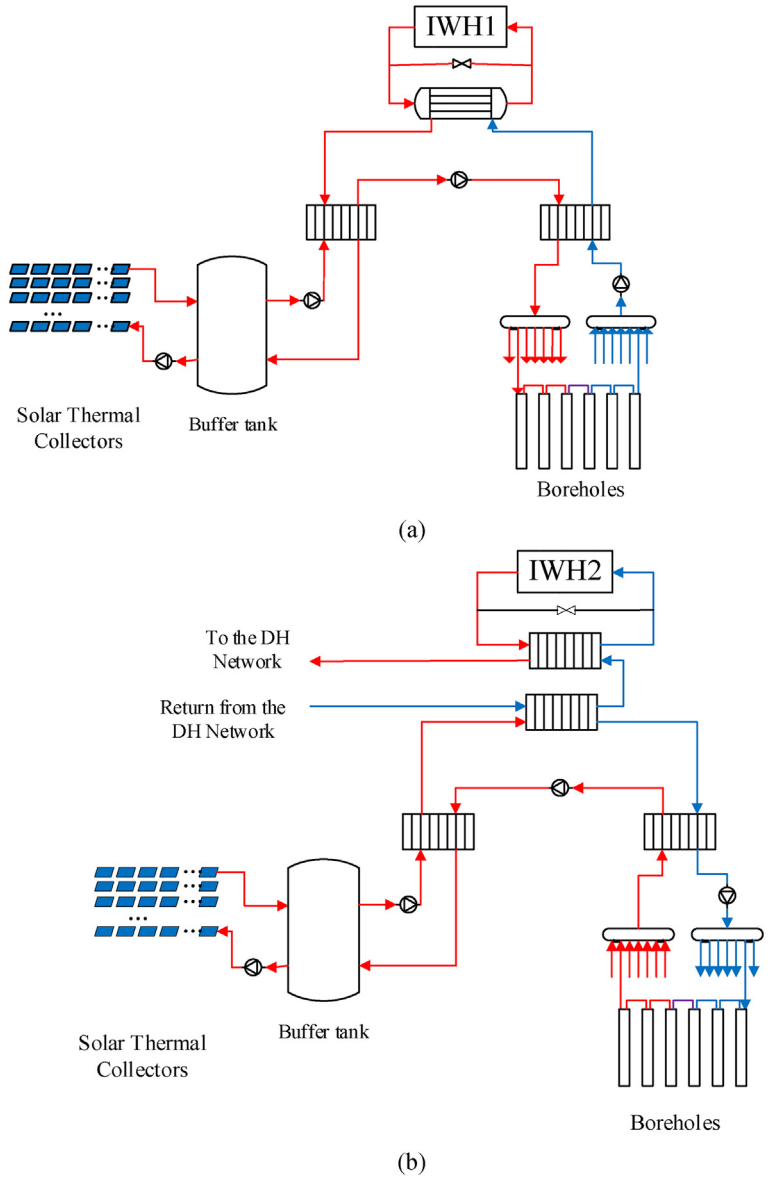

Fig. 1. System diagram for (a) non-heating season and (b) heating season.

as possible. In addition to the system goals, the overall BTES system efficiency is influenced greatly by the thermal transport behavior of borehole heat exchangers (BHE). Zhu et al. [21] investigated the transient thermal performance of a vertical double U-tube BHE operated under different operation conditions including flow rate and charging temperature. The results indicated that the charging temperature had a larger influence than the flow rate on lifting soil temperature. Luo et al. [22] compared three operation strategies of BHEs for a large-scale hybrid ground source heat pump (GSHP) system. The research showed that, for the large-scale hybrid GSHP system, operating all BHEs at the same time would result in a slightly higher heating and cooling efficiency but much higher operating costs compared to the other two strategies that only one or several zones of the BHEs were under operation. As such, operations of BHEs in a BTES should be carefully investigated. Based on these goals and the existing literature regarding operation strategies of BHEs, three operation strategies of the BTES subsystem for the heating season were defined:

1) *Overall control.* The whole BTES subsystem runs at a fixed mass flow rate in the main pipe. Overall operation strategy is a conventional operation strategy. The simplicity of its control system and hydraulic system is its advantage. However, due to large soil thermal inertia, the outlet water temperature of BTES tends to decrease gradually in the heating season. Therefore, extra heat may be required from the back-up IWH subsystem in later period of the heating season.
2) *Zonal control.* The BTES subsystem is divided into several parallel zones; six zones in this pilot system. To achieve a relatively stable outlet temperature, the BTES subsystem is operated zone by zone at a fixed mass flow rate in the main pipe. Only one zone is under operation when the heat season starts. All other zones are switched off. Storage temperature of the BTES subsystem is monitored. When the monitored storage temperature is below a certain temperature set-point, the current operation zone is switched off and another zone is activated. Once the monitored temperature of all

BTES zones are below the setpoint, the BTES subsystem switches to the overall control mode. The same operation strategy applies to all BTES zones until the end of the heating season. Then, all zones are under operation throughout the non-heating season to maximize heat injection to the BTES.

3) *Time-scheduled combined control*. Inspired by [22,23], this operation strategy is designed to better allocate extracted heat according to heating demand/outdoor temperature. This operation strategy combines the overall operation strategy and the zonal operation strategy. It allows to take advantage of both methods. The BTES subsystem operates by the zonal operation strategy in the beginning and the end of the heating season when heating demand is generally low. The overall control applies in the rest of the heating season when outdoor temperature is relatively lower and heating demand is higher than in the beginning and the end of the heating season.

It is not straightforward to decide on which operation strategy to use for the system due to the complex thermal behavior of the BTES and the dynamic interaction between heat demand and heat sources. Therefore, the performance of the system needs to be investigated in detail for the various operation strategies. To understand the performance of large-scale BTES, it is crucial to perform a long-term performance assessment [24]. One way would be to perform long-term experiments on the actual system. However, this is time consuming and expensive. Furthermore, for large installations, it is not practical to use experimental analysis in order to test the operation strategies under various scenarios (e.g. weather conditions or variations in heat demand). This drawback may be overcome by small-scale experimental studies combined with modeling and simulation. Experimental results can be used to validate simulation models [24–26] and the models can be used to investigate the performance of the operation strategies under various scenarios. The latter approach is adopted in this research to investigate the most appropriate operation strategy for the BTES in the Chifeng district heating system.

Several studies adopt modeling and simulation methods to evaluate the performance of BTES integrated DH systems. Ciampi et al. [27] conducted a thermo-economic analysis in TRNSYS for a small DH system with seasonal BTES and solar collectors. The study investigated the influence of the sizing of the components (area of solar collectors and volume of storage) on primary energy consumption, carbon emissions and operating costs. Elhashmi et al. [4] performed a parametric simulation using a one-month time-step to evaluate the economic performance of a district solar BTES system for multi-family residential buildings. Existing studies also conducted multi-objective optimization to optimize the environmental and economic performance of BTES integrated DH systems considering different locations [28] and different environmental and economic scenarios [11]. However, little attention has been paid to model validation of the simulated BTES integrated DH systems. In addition, few studies have investigated the operation strategies of BTES in DH systems.

Thus, this paper presents a modeling and simulation method that supports energy performance assessments and operation strategy investigation of BTES in the Chifeng district heating system. The validity of the BTES model is discussed extensively. In Section 2, various methods to model BTES are reviewed and the motivation for our choice of model is explained. Section 3 is concerned with the measurements used in this study. The fourth section describes the models and their validity. Results are presented and discussed in Section 5. The paper closes in Section 6 with conclusions and directions of future work.

2. Overview of modeling and simulation methods for BTES

A number of design tools and models have been developed to account for the transient behavior of borehole heat exchangers [29–33]. These models are mainly numerical models that are based on finite element method or finite volume method in 2D or 3D forms. In this respect, numerical models are able to account for the exact borehole geometry, groundwater flow effect and transient heat transfer effect. The main challenge of using these models is the high computational workloads, particularly for large scale borehole heat exchanger arrays applied in BTES systems [29,34].

On the other hand, analytical methods require lower computational workloads [29]. Analytical models describe a BHE as either a line source or a cylinder source, providing the temperature response to a uniform heat pulse. Analytical models are often applied on a single borehole. Infinite line source (ILS) models are the simplest analytical models for BHE. ILS models treat the BHE as an infinite line source that continuously generates heat from time zero. Thermal conduction is the only heat transfer process considered in ILS models. The ILS model was first developed by Whitehead [35] and further developed by Ingersoll and Plass [36] and Carslaw and Jaeger [37]. Mogensen [38] modified the ILS model to better represent a U-tube BHE. Infinite cylinder source (ICS) models share the same principle with ILS models. The only difference, as indicated by their names, is that the heat source is assumed to be a cylinder with an infinite length instead of an infinite line. ICS models have different forms according to the material inside the cylinder (borehole). Readers are referred to [37] for detailed descriptions and applications of the different forms. One common drawback of ILS and ICS models is that they treat the heat transfer from the BHE to the surrounding ground in only one dimension, i.e., the radial direction. The axial temperature gradients are neglected, although these would start to be significant when BHEs are operated for longer than a year [39]. Finite line source (FLS) models should be used when the design period is greater than a year. FLS models provide the temperature response to a finite line source with a length of L and located at a distance of D from the ground surface. FLS models can also evaluate the thermal influence of one borehole on another. FLS models come in several forms and their use depends on whether they are to be applied on single or multiple boreholes. In the case of multiple boreholes, FLS can also have different forms if the boreholes have different values for L and/or D. For BTES applications, boreholes often have the same length and are buried at the same depth. In this respect, the FLS model developed by Claesson and Javed [40] would be the best fit.

As illustrated above, analytical models provide the solution of a constant heat injection or extraction load on BHEs. However, in practical applications of BHEs, especially for BTES, the heat injection or extraction load often changes over time. To better represent the time-varying heat load, response function (g-function) models based on the superposition principle were developed. The application of the superposition principle was first introduced by Claesson and Dunand [41]. The superposition principle deals with the linear heat conduction equation and boundary condition while neglecting nonlinear terms in ground heat transfer, such as freezing/thawing, groundwater flows, radiative heat exchange at the surface, etc. Superposition can be applied both temporally and spatially. The analytical g-function model, originally developed by Eskilson [42], is the most widely used g-function model for borehole fields. The g-function converts the temperature response of the borehole field into a dimensionless form in response to a step heat input. It is only valid for time-steps longer than three to six hours for a typical borehole, which is larger than the normal time-step (one hour) in building performance simulation. The original g-function model

has been further improved by Yavuzturk and Spitler [43] to manage short time steps and also to take into consideration the thermal capacitance and resistance of individual borehole elements.

Various borehole models have been implemented in TRNSYS. The most common model is the Duct Heat Storage (DST) model. The DST model treats the thermal process in a BTES as two parts, i.e., a global problem that deals with the heat transfer between the boreholes and the surrounding ground, and a local problem that deals with the heat transfer around the pipes in the boreholes. The DST model adopts the spatial superposition principle to solve the heat transfer in BTES. A limitation of the model is that it is only applicable for cylinder-shaped BTES with vertical symmetry axis and uniformly placed ducts [44]. It adopts a steady-flux regime which assumes a constant heat injection/extraction rate. Thus, the DST model ignores the dynamics of the heat exchange between the borehole wall and the heat carrier fluid. It also overestimates the long-term temperature response [45]. In order to simulate user-defined borehole configurations and obtain short-term and long-term accuracy for yearly-based simulations, Picard and Helsen [45] developed a hybrid step-response model (HSRM) for borehole field heat exchangers in Modelica. Another advantage of the HSRM model over other models is the possibility of implementation in multiple borehole simulations. A detailed comparison between the DST TRNSYS (Type557) model and the Modelica HSRM model follows below.

2.1. TRNSYS Type 557 vs. Modelica HSRM borefield model

The TRNSYS Type 557 implements the DST model which is only applicable for cylindrical borehole configuration with a uniform borehole distribution. The exact shape and position of each borehole can be described in the Modelica HSRM Borefield model. Another main difference between the two models is that the TRNSYS Type 557 model does not consider the dynamic behavior of the heat transfer from the heat carrier fluid to the borehole wall, while the Modelica HSRM Borefield model does. The TRNSYS Type 557 model can specify thermal properties for insulation materials on top of borefields, while the Modelica HSRM Borefield model assumes an adiabatic boundary condition for the top of borefields. The Modelica HSRM model supports multiple storage module connections, which is important if comprehensive operation strategies are considered. As for the outputs, the main difference between the two models is the index for the borefield temperature. The TRNSYS model provides an average borefield temperature. This is important if seasonal change in soil temperature is regulated by local standards or laws. The Modelica HSRM Borefield model provides average borehole wall temperature instead, which is more similar to the temperature of the heat carrier fluid. The main considered features and available outputs for the two BTES models are summarized in Table 1.

It should be noted that the heat loss is calculated in the short-term response part of the HSRM model. The heat transfer between a borehole and the surrounding ground is calculated by a resistance-capacitive network. An undisturbed ground temperature (10.6 °C in this case) is defined and is located 3 m away from the borehole wall. The ground is divided in to several layers and each layer has its own resistance and capacitance in the model.

2.2. Model selection

The pilot system presented in this paper adopts a noncylindrical, hexagonal-shaped borefield. The BTES model should represent the physical shape of the borefield as designed. In addition, as illustrated at the end of Section 1, the main objective of this research is to investigate operation strategies of BTES in the Chifeng district heating system to reduce the usage of the back-up IWH subsystem (IWH2) in the heating season as much as possible. The borefield is divided into several zones in two of the operation strategies. Therefore, the BTES model should be capable of connecting multiple storage modules.

On the basis of the above, we concluded that the Modelica HSRM model was required in order to be able to investigate a system with multiple boreholes. Therefore, the Modelica HSRM model was used to investigate the performance of the operation strategies. Section 4 presents the results of an inter-model comparison validation study between the TRNSYS Type 557 and the HSRM model.

Table 1
Summary of the features of the TRNSYS Type 557 model and the Modelica HSRM Borefield model.

	TRNSYS Type 557 model	Modelica HSRM Borefield model
Considered Features		
Top Insulation	Y	N
Heat losses	Y	Y[1]
Dynamics of the borehole heat exchanger	N	Y
Number of boreholes in serial	Y	Y
Number of boreholes in parallel	Y	Y
Contact heat resistance at U-tube surfaces	Y	N
Change flow direction	Y	Y
Connect multiple storage modules	N	Y
User-defined boreholes' distribution	N	Y
User-defined borefield shape	N	Y
Available Outputs		
Average borefield temperature	Y	N
Borehole wall temperature	N	Y
Outlet water temperature and mass flow rate	Y	Y
Heat losses to the air and the surrounding ground	Y	N
Storage internal energy changes	Y	Y

[1] Considered in the short-term thermal response model.

3. Measurements and monitoring of the pilot system

The measurements of the Chifeng pilot system consist of two parts. First, a soil thermal response test was conducted to obtain the on-site soil thermal properties (the soil thermal conductivity and thermal capacity). Three boreholes were drilled in different locations on-site and U-tubes were inserted in the boreholes as heat exchangers. Fig. 2 depicts the system schematic of the soil thermal response test. Water was heated by an electric heater and then injected into the borehole heat exchanger. Flow rate, inlet

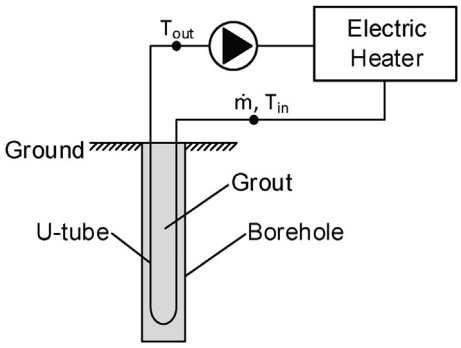

Fig. 2. System schematic of the soil thermal response test.

water temperature and outlet water temperature were measured and logged every minute for 48 h. The measured data from the soil thermal response test were then applied in calculating the soil properties. The calculation for the soil properties is described in Section 4.2.

The living laboratory is equipped with various sensors in order to perform measurements during operation of the system. The volumetric flow rate and the water temperature were monitored and logged on a minute-basis in the distribution pipes connecting the different system components. The positions of the sensors are shown in the system scheme in Fig. 3. Each black dot represents a sensor. Temperatures (T_{in1}, T_{out1}) are measured in the main supply and return pipes, as well as in separate pipes before the hydraulic manifold (T_{out2}). The system operational measurements were performed from 28-Aug-2016 until 18-Apr-2017.

4. Model validation and simulation setup

As mentioned in Section 2, this research uses the Modelica© language to model the solar-IWH STES system. Modeling and simulation were executed in Dymola (Version 2018), a commercial Modelica-based modeling and simulation tool. The modeled system is composed of several model components from open source libraries. The Modelica Standard Library, Buildings Library and IDEAS Library are used in this research.

4.1. Model description

As the solar-IWH STES system consists of four subsystems, the model for the system also splits into four sub models; namely, the solar thermal sub model, the borehole thermal energy storage sub model, the industrial waste heat sub model and the district sub model. The layout of the modeled system in Dymola is described in Appendix B. Main model components and their related libraries for each subsystem are listed in Appendix C. Details of the model can be found in previous research [46].

4.2. Calculation for soil thermal properties

Previous research shows that the soil thermal properties (thermal conductivity λ_{soil} and specific heat capacity c_{soil}) have a significant influence on the energy performance of the STES system [46]. Therefore, the data quality of these sensitive inputs requires special attention in order to achieve a reliable result in the empirical validation test. As upper mentioned in Section 3, this research conducted a thermal response test to determine an effective thermal conductivity over the whole length of the BHE. The thermal responses of the boreholes were evaluated during injection of constant heating power. Thermal conductivity and specific heat capacity of the soil were determined through the procedure shown in Fig. 4. Table 2 lists the calculated soil parameters according to the thermal response test. These values were used in the BTES models. It should be noted that data from one of the three test boreholes was considered to be unreliable. The calculated thermal conductivity is only 0.512 W/m·K. Therefore the unreliable data was omitted from the analysis. Only data from two test boreholes are listed in Table 2.

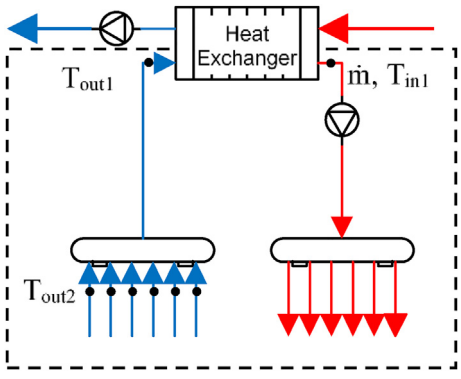

Fig. 3. The scheme of the BTES subsystem with the position of sensors.

4.3. Model validation

4.3.1. Inter-model comparison

The following section presents the (simulation) experimental design of the inter-model comparison. Two BTES models are compared, i.e. the DST model implemented in TRNSYS and the HSRM model implemented in IDEAS Modelica library. Two groups of cases were tested under different parameters to analyze the effect of borehole heat exchangers' aggregation. The first experimental group (SExp 1, 2 and 3) was designed to test a single borehole. The other experimental group was for a borehole field with 468 boreholes. Different operational conditions were considered for each case, the preheating operation (inject heat in the first year), the summer operation (inject heat under the desired condition) and the winter operation (extract heat). Table 3 lists the parameters of the simulation experiments. Since the TRNSYS-DST model does not allow multiple storage modules to be connected, the overall operation strategy was chosen to operate the BTES subsystem for the inter-model comparison.

Fig. 5 depicts the simulated outlet water temperature (as shown in Fig. 5 (a)) and the injected heat (as shown in Fig. 5 (b)) by the

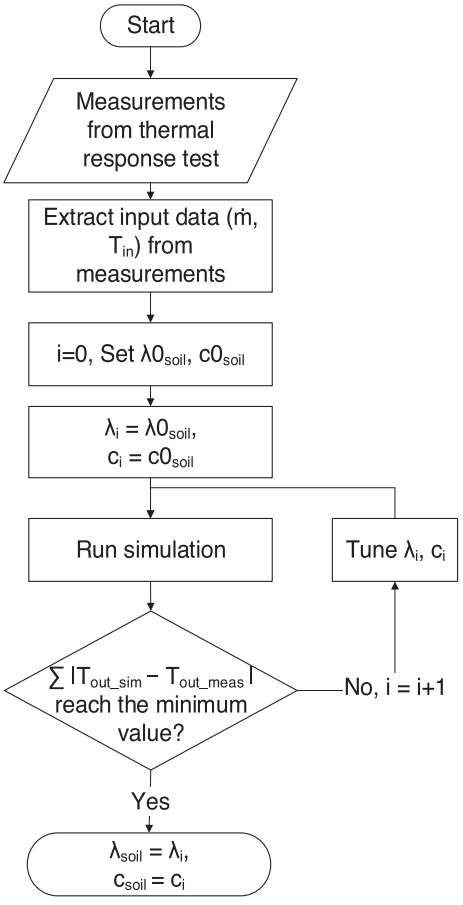

Fig. 4. Procedure of soil property calculation.

Table 2
Calculated soil parameters according to the thermal response test.

1# BH		2# BH	
λ_{soil}	ρc_{soil}	λ_{soil}	ρc_{soil}
W/m·K	10^6J/m^3·℃	W/m·K	10^6J/m^3·℃
1.4544	1.875	1.0193	1.941

two models for the case SExp 1. Blue lines represent simulation results obtained by the TRNSYS model and the yellow lines represent simulation results obtained by the Modelica model from IDEAS library. Results from both models show the outlet water temperature increased rapidly in the beginning of the heat injection. With 75 °C water injected into a single borehole, the outlet water temperature increased by 50 °C and reached 62 °C within the first 24 h. It then gradually increased to 67 °C by the end of heating season.

As for the comparison between the two models, the TRNSYS model predicted higher outlet temperature and thus less injected heat. The difference in aggregated injected heat was 5% and the coefficient of variance of the root mean square error (Cv(RMSE)) of injected heat was 6.5%. As shown in Fig. 5 (c), only in the first few hours, the TRNSYS model predicted much higher outlet temperature than the Modelica model from IDEAS library. Then, the difference reduced to 1 °C after 8-hour operation. The average hourly temperature difference of the entire heating season was 0.4 °C.

Fig. 6 depicts the simulated outlet water temperature and the injected heat for the case SExp 2. This case represents heat injection for a single borehole under desired operational condition. Similar phenomena can be found as in the case SExp 1. Due to a higher initial soil temperature, the outlet water temperature rose more slowly and the injected heat was less compared to the first-year-injection case (SExp 1). The outlet water temperature reached around 71 °C for both models. The difference in the simulation results between the two models was also smaller. The difference in aggregated injected heat was 4% and the Cv(RMSE) of injected heat was 5.8%. The average hourly temperature difference of the entire heating season was 0.2 °C.

As for the single-borehole heat extraction case, initial soil temperature was assumed to be 55 °C, based on design documents. Stored heat was extracted with a 25 °C water inlet. As shown in Fig. 7 (a), outlet water temperature declined drastically in the first four hours. Water temperature dropped from 55 °C to 33 °C. As the heat extraction proceeded, outlet water temperature slowly reduced to 28 °C and 29 °C, respectively, according to the prediction by the TRNSYS and the Modelica models.

Regarding the borehole field cases, the differences between the two models were more significant than in the single borehole cases. In addition, contrary to the single borehole cases, the TRNSYS model predicted lower outlet water temperature and higher injected heat for the borehole field experiments. Take the preheating operation as an example, the predicted outlet water temperature and the injected heat are shown in Fig. 8. What can be seen in this figure is the rapid increases of the outlet water temperature predicted by the Modelica-IDEAS model. The TRNSYS model predicted a much slower rise in outlet water temperature in the first few days and a slightly faster rise in the rest of the running time. The difference in aggregated injected heat predicted by the two models was 12% and the Cv(RMSE) of injected heat was 12.5%. The average hourly temperature difference was 3.6 °C. The indices measuring the differences between simulation results from the two models for the other two cases are listed in Table 4.

In short, for the single borehole cases, the difference in simulated injected/extracted heat was around 5%. The difference in simulated outlet water temperature was much larger in the first eight hours, and then reduced to less than 1 °C. The average temperature differences were less than 0.5 °C for the three single borehole cases. For the borehole field cases, the difference in simulated injected/extracted heat was larger than in the single borehole cases but less than 13%. The TRNSYS model predicted lower temperature and larger injected/extracted heat. The differences in average hourly temperature were less than 4 °C for the three borehole field cases. The results reflect that the two models treat the thermal response in borefields differently.

4.3.2. Empirical validation

To further assess the credibility of the BTES model, an empirical validation test was conducted. The test used the calculated soil parameters to simulate the BTES performance and compared the results with measurements. The model for the empirical validation test consisted of a timetable component to read inputs, a pump component, a BTES component and a temperature sensor component for output. The timetable component was used to read the measured flowrate and temperature as inputs. The pump component describes an ideal mass source with prescribed mass flow rate and prescribed temperature defined in the timetable component. The HSRM model implemented in IDEAS Modelica library was adopted to model the BTES. Finally, the fluid temperature leaving the borefield was obtained through the temperature sensor component and compared with measurements.

Fig. 9 (a) compares the simulated and measured outlet water temperature from the BTES subsystem throughout the 233-day operation. The time interval is one minute, in compliance with inputs. There are several periods when one or more temperature sensors were defective. The defection periods were days 5–10, 14–15, 16–17, 21–22, 61–62, 101–103, and 209–213. Data from the defection periods were excluded for comparison, thus lines in Fig. 9(a) are discontinuous. The results show that the model succeeded in simulating the pattern of the fluctuation across the measurements except for the first five days of operation. The discrepancies between the simulation and measurements reach up to 20 °C in the first five days. However, it is worth noting that the system is under commissioning operation in the first five days, therefore the measurements may not be reliable. The differences mainly range from 0 °C to 3 °C. This range covers more than 80% of the data points. The model predicted higher temperatures than the measurements throughout the entire system operation period except for several spikes. The sudden drops in outlet water temperature occurred when the copper plant was under maintenance, thus no IWH source was available at that time. The model

Table 3
Parameter settings for inter-model comparison on BTES models.

No.	Initial T_{soil} (°C)	Number of the boreholes	Inlet water temperature (°C)	Flow Rate (kg/s)	Notes
SExp 1	12	1	75	0.167	Injection, first year
SExp 2	40	1	75	0.167	Injection, desired condition
SExp 3	55	1	25	0.167	Extraction
SExp 4	12	468	75	13	Injection, first year
SExp 5	40	468	75	13	Injection, desired condition
SExp 6	55	468	25	13	Extraction

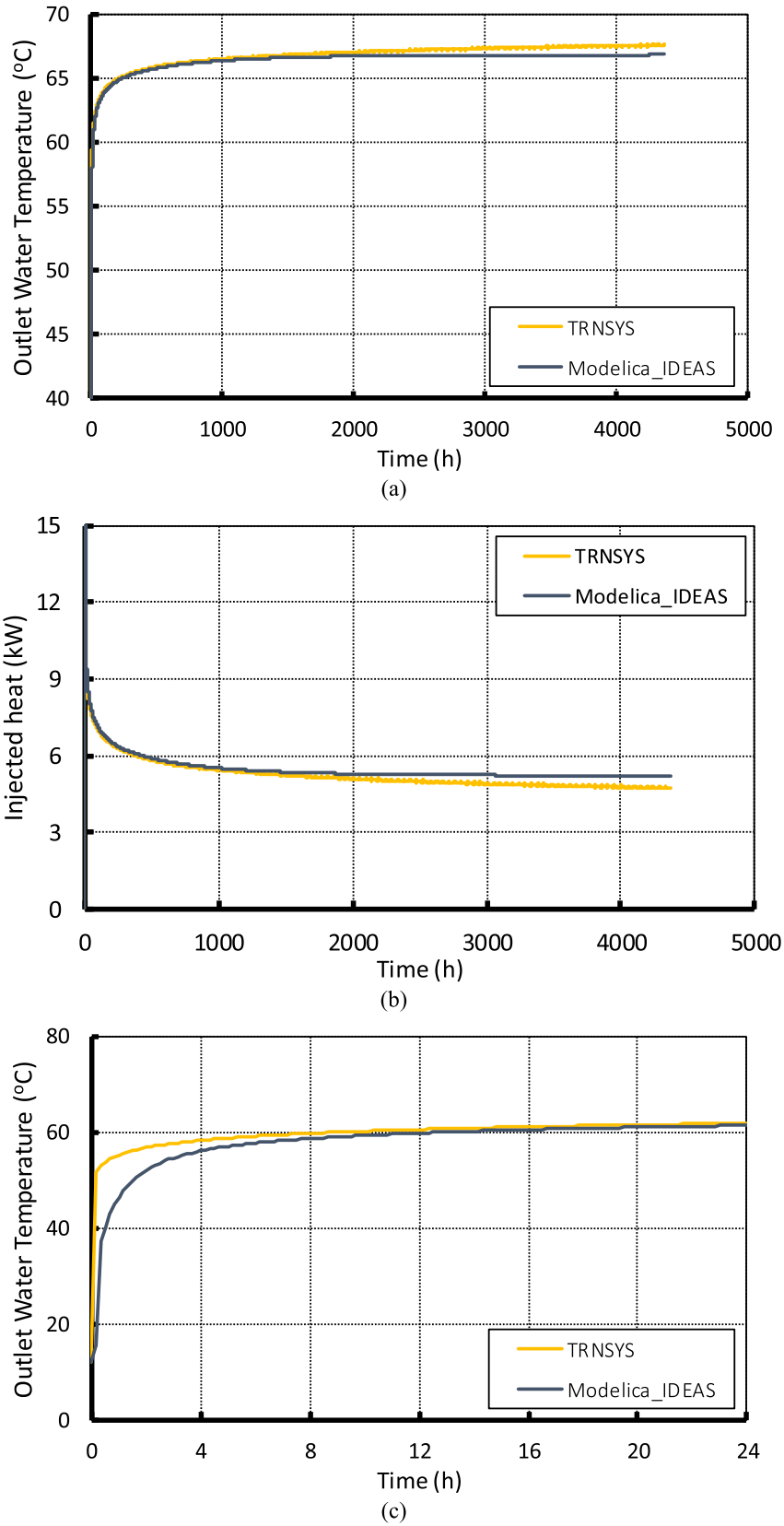

Fig. 5. The comparison of the two models on outlet water temperature (a) and injected heat (b) for SExp 1 during a non-heating season and outlet water temperature during the first 24 h (c).

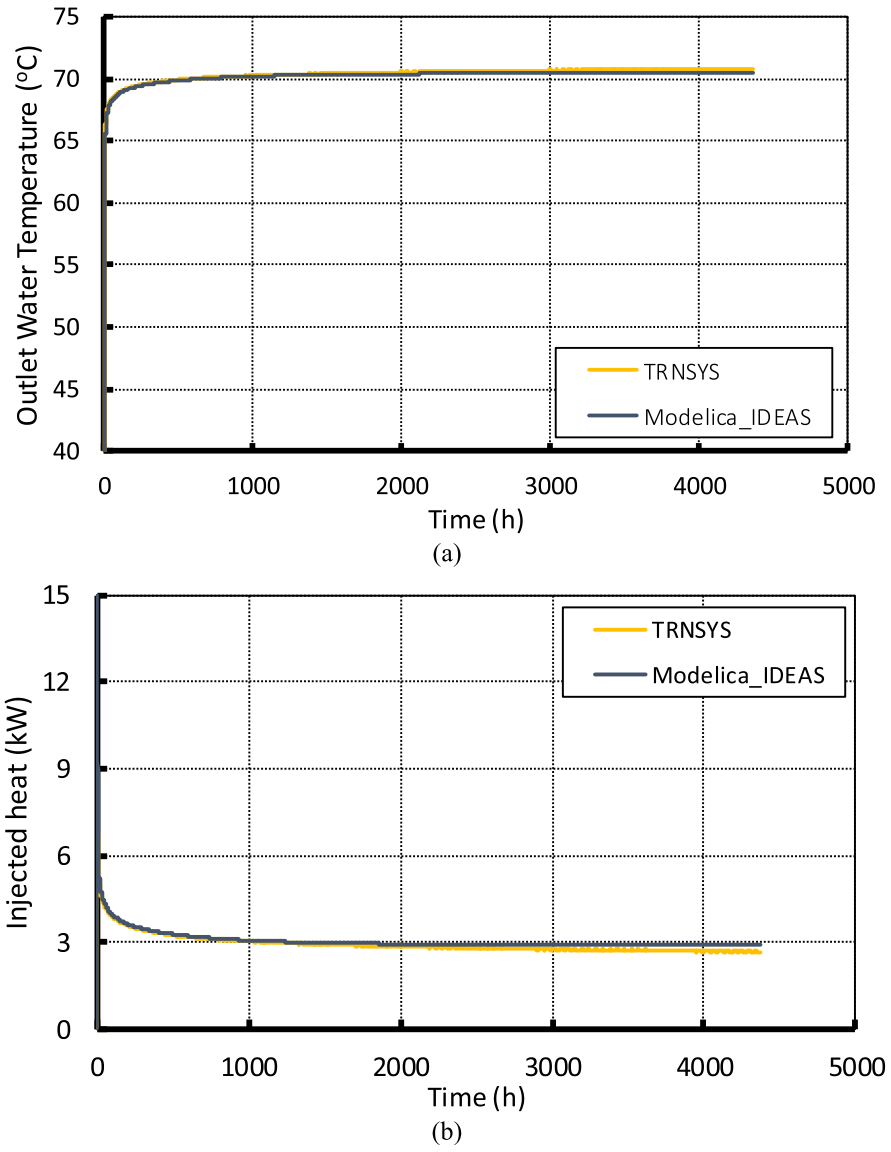

Fig. 6. The comparison of the two models on outlet water temperature (a) and the injected heat (b) for SExp 2.

predicted more significant changes when maintenance occurred. Fig. 9(b) displays the variation in temperature difference by means of a boxplot. The central mark in red represents the median, and the bottom and the top edges of the blue box indicate the 25% and 75% percentiles. The whiskers extend to the largest datum within the 1.5 interquartile range (IQR) above the 75% percentile and the lowest datum within the 1.5 IQR below the 25% percentile. All other data beyond the range between the whiskers are considered as outliers and are not shown in the boxplot. The differences between the simulation and the measurements reduced after 110 days of operation. The median of the temperature differences was 2.0 °C in the first 110 days and reduced to 0.8 °C for the following period.

Fig. 10 provides the correlation between simulated and measured injected heating energy on an hourly basis. As expected, most points fall below the diagonal line (in black), which indicates that the simulated injected heating energy is smaller than the corresponding measurements. This is simply because the model predicts higher outlet water temperature and the other variances affecting the injected heating energy, the flow rate and the inlet water temperature are the same as for the measurements. A simple linear regression was performed, shown by the red line in Fig. 10. The square of the correlation coefficient (r^2) is 0.974, which indicates the measurements and the simulation results have a strong linear relationship. Thus, the precision of the model prediction in injected heating energy is quite high. The regression function is shown in Fig. 10. If predicted heating energy from BTES subsystem is of interest, then the results can be modified by applying the inverse of the regression function.

To quantify how the predictions of the models deviated from the measurements, proper statistical indices should be applied. Commonly, the mean bias error (MBE) and the coefficient of variation of the root-mean-square error (Cv(RMSE)) are used in building energy modeling [47]. MBE is calculated as the sum of the difference between the measurements and simulated data at the

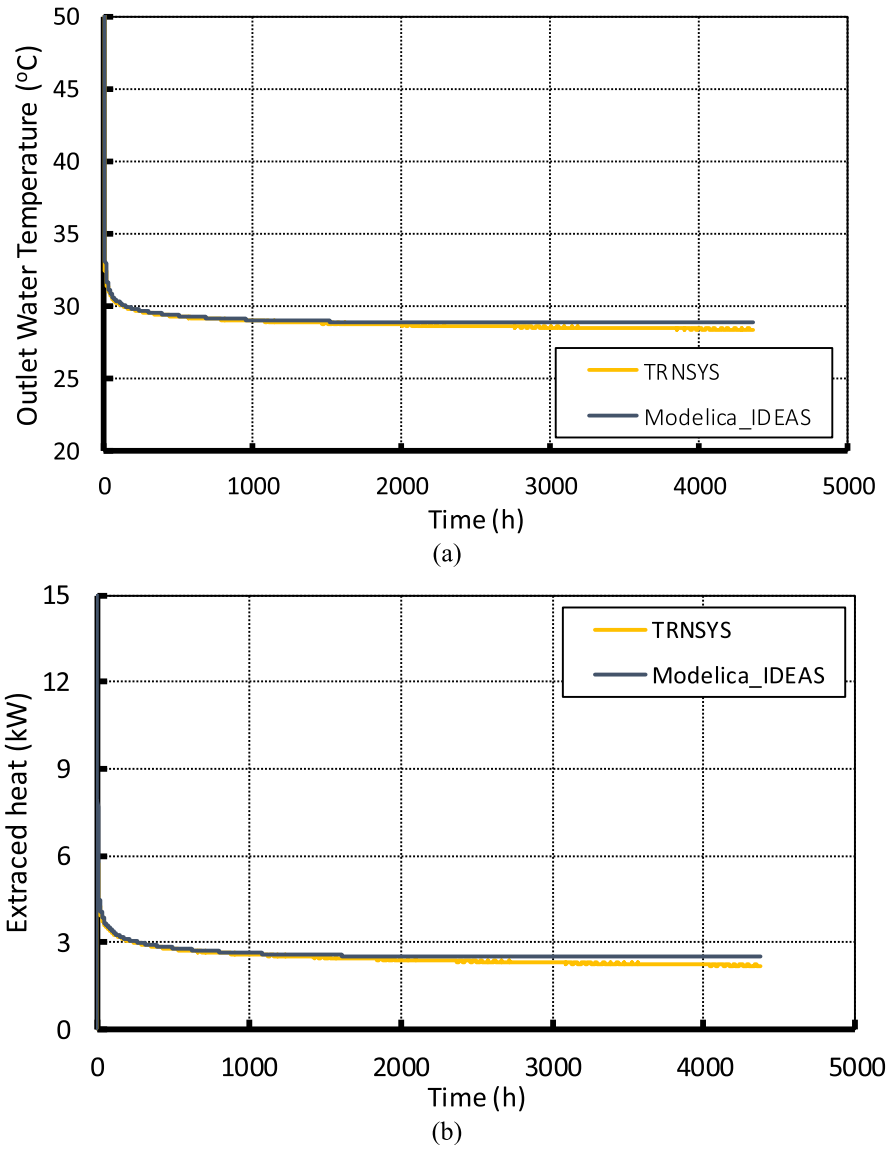

Fig. 7. The comparison of the two models on outlet water temperature (a) and the extracted heat (b) for SExp 3.

simulated time intervals (hour in this research) and normalized by the sum of the measurements.

$$\mathrm{MBE} = \frac{\sum_{i=1}^{n}(y_{sim,i}-y_{mea,i})}{\sum_{i=1}^{n} y_{mea,i}} \quad (1)$$

where:

$y_{sim,i}$	is the simulated data point at the time interval i
$y_{mea,i}$	is the measured data point at the time interval i
n	is the number of data points

MBE should be interpreted with caution since positive and negative errors will cancel each other out. Therefore, the Cv(RMSE) is introduced to assist the assessment. The root-mean-square error (RMSE) or root-mean-square deviation (RMSD) represents the quadratic mean of the differences between the measurements and simulated data. The Cv(RMSE) is the RMSE normalized by the mean value of the measurements. The Cv(RMSE) is calculated as shown in Eqs. (2) and (3)

$$\mathrm{RMSE} = \sqrt{\frac{\sum_{i=1}^{n}(y_{sim,i}-y_{mea,i})^2}{n}} \quad (2)$$

$$\mathrm{Cv(RMSE)} = \frac{\mathrm{RMSE}}{\bar{y}_{mea}} \quad (3)$$

where:

$ymea$	is the mean value of the measurements
n	is the number of data points

The limit threshold is defined slightly differently among standards/protocols [47]. This study adopts the strictest thresholds from the International Performance Measurements and Verification protocol (IPMVP) [48]. IPMVP defines the thresholds as ± 5% for the MBE and 20% for the Cv(RMSE). MBE of the outlet water temperature is 4% and Cv(RMSE) is 7.9%. As for the hourly heating energy injection

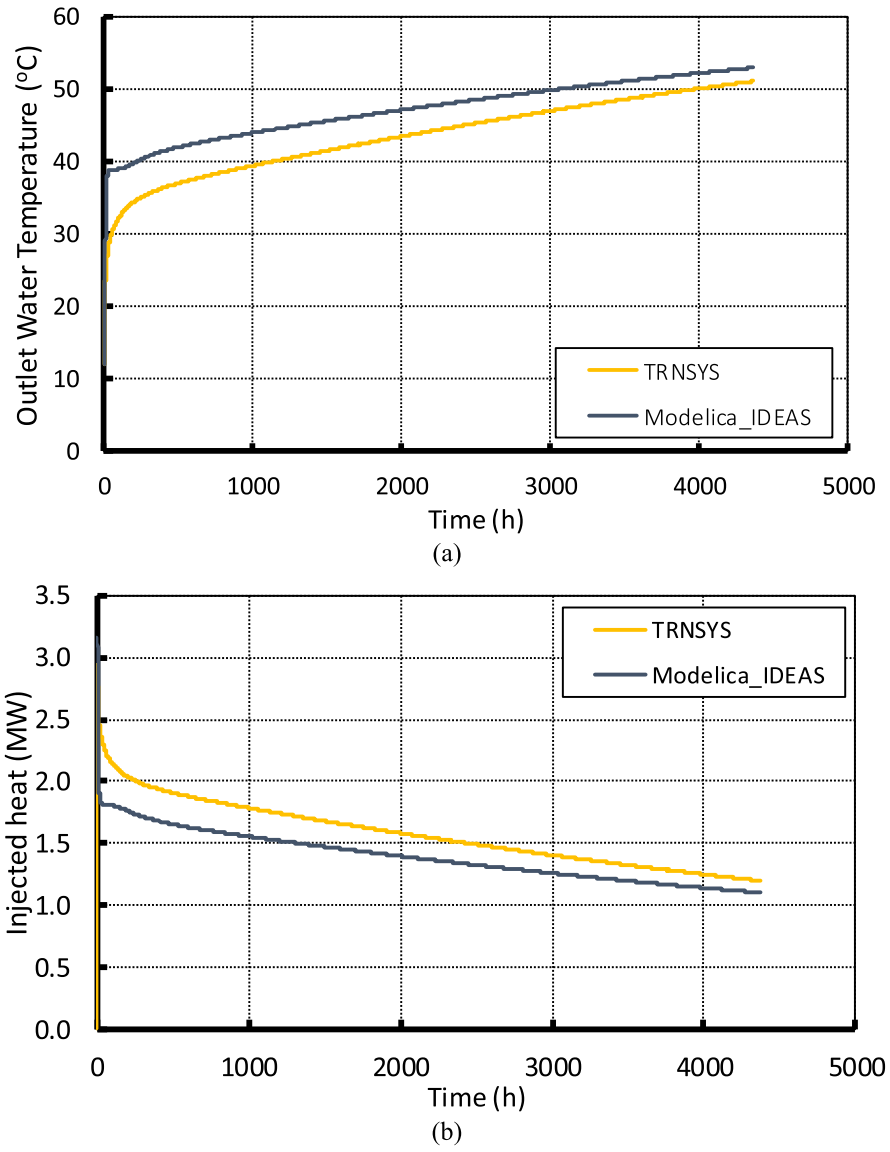

Fig. 8. The comparison of the two models on outlet water temperature (a) and the injected heat (b) for SExp 4.

Table 4
Differences between simulation results from the two models for the borehole field cases.

Cases	Aggregated injected/ extracted heat (%)	Cv(RMSE) of injected/ extracted heat (%)	Average hourly temperature (°C)
SExp 4 – first-year injection	12	12.5	−3.6
SExp 5 – injection under desired condition	12	13.0	−2.2
SExp 6 – extraction	11	11.9	1.6

to the BTES, the values are −4.9% for MBE and 9.7% for Cv(RMSE). All of the values are lower than the threshold in IPMVP [48].

Discrepancy between the measured and the simulated data may be caused by two main reasons; simplifications and assumptions during modeling, and/or uncertainties in measurements. The following content gives an insight into the measurement uncertainty. The measurements used for the test covered 7 months and 21 days, from 28-Aug-2016 to 18-Apr-2017. Fig. 11 shows the measured water temperature in the six separate return water pipes (T_{out2} in Fig. 3) before the manifold. Due to page limitation and for a better visualization, only the data of two typical weeks in the third month and two typical weeks in the sixth month are presented here. Water temperature did not distribute evenly among the six parallel storage partitions. The differences between the highest and the lowest was around 5 °C in the first three months and reduced to 1 °C from the fifth month of system operation. The average value of the temperature differences among the six pipes was about 1.5 °C.

5. Performance assessment of the three operation strategies

The results of the performance assessment are presented in this section. In the first subsection, the six scenarios are defined (two building insulation levels and three weather scenarios). In the second subsection, the performance of the studied system with the three BTES operation strategies under the six scenarios are assessed and discussed based on the simulation results.

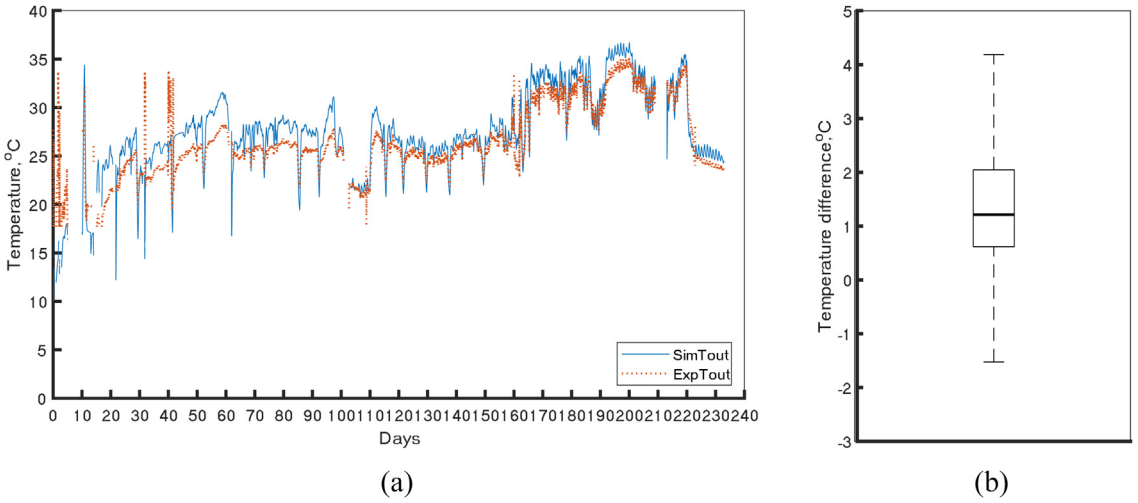

Fig. 9. Comparison between simulation and measurements of outlet water temperature (a) and the variation in temperature difference (b).

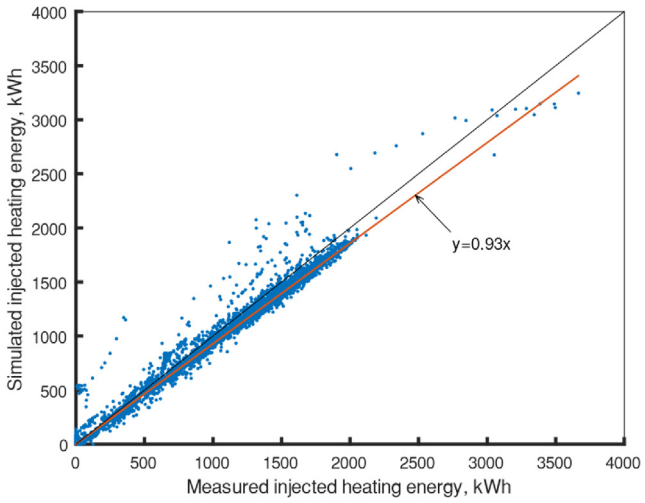

Fig. 10. Correlation between measured and simulated hourly injected heating energy.

5.1. Scenario definition

Different building insulation levels and weather conditions were considered as scenarios for the performance assessment. The current building insulation level is labelled the *as is* scenario. The U value of external walls is 1.28 W/m^{2}K and the U value of windows is 3.26 W/m^{2}K. Another scenario for building insulation level, labelled *current regulation*, is covered considering possible renovation in the future. The *current regulation* scenario is set to examine buildings of which the thermal properties are in compliance with the current design standard for energy efficiency of public buildings [49]. As regulated in the standard, U values of external walls, floors, windows and roofs are 0.43 W/m^{2}K, 0.43 W/m^{2}K, 2.3 W/m^{2}K, 0.35 W/m^{2}K, respectively. The weather condition scenarios cover standard weather, extreme weather and mild weather. The weather files are derived from Chinese Standard Weather Data (CSWD), developed by Department of Building Science and Technology at Tsinghua University and China Meteorological Bureau [50]. The weather files are developed for use in simulating building heating and air conditioning loads and energy use, and for calculating renewable energy utilization. The typical year data (standard), extreme years for maximum solar radiation (extreme) and minimum solar radiation (mild) for Chifeng city are adopted in this research.

5.2. Performance assessment of the solar-IWH STES system with different BTES operation strategies

The three operation strategies of the BTES subsystem were tested using the validated model. First, the simulation results of the reference case are described and the performance of the system is analyzed. Next, the comparison among the three operation strategies on the system performance is presented.

5.2.1. Reference case

Reference case represents the studied system with the *Ref* BTES operation strategy (overall control) under scenario 1 (*as is* building insulation level with *standard* weather). Fig. 12 depicts the daily heat balance of the reference case at the subsystem level. The positive values in the figure represents a subsystem that supplies heat and the negative values represents a subsystem that consumes heat (DH) or that is charging (BTES). In the non-heating season (from day 106 to day 288), there is no heating supplied by the solar-IWH STES system. The system is running to charge the BTES. The total injection heat of the BTES subsystem was 1.91 GWh. The injection heat was mostly provided by the IWH subsystem (1.86 GWh) and the STS only played a minor role. The graph shows that the daily injected heat gradually decreases along time. This phenomenon indicates that the BTES was reaching its capacity.

In the heating season, the total building heating demand was 2.78 GWh, depicted by the blue area in Fig. 12. The BTES subsystem provided 2.22 GWh of heating in the heating season. It covered 80% of the total heating demand; this made the BTES subsystem the primary heating supply source of the system. The rest of the heat was supplied by the IWH subsystem (0.63 GWh) and the STS subsystem (0.05 GWh) respectively. It can be seen that the BTES subsystem played a more important role in the beginning of the heating season (roughly the first month, from day 289 to day 318). In this period, the BTES subsystem covered 97.1% of the heating demand. Almost no heat was required from the IWH subsystem. This is due to the fact that the heating demand was relatively low, while the state-of-charge of the BTES was relatively high right after the injection period in the non-heating season. As the heating demand increased along the heating season, the share of the energy supplied by the IWH subsystem increased as well. When the heating season reached its end, the system performed

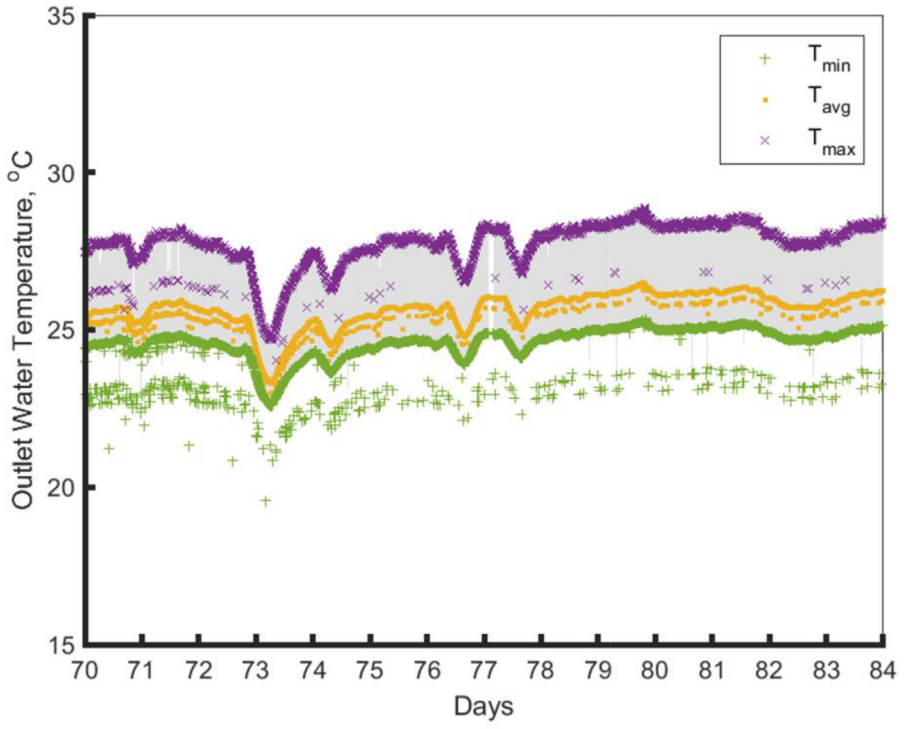

(a)

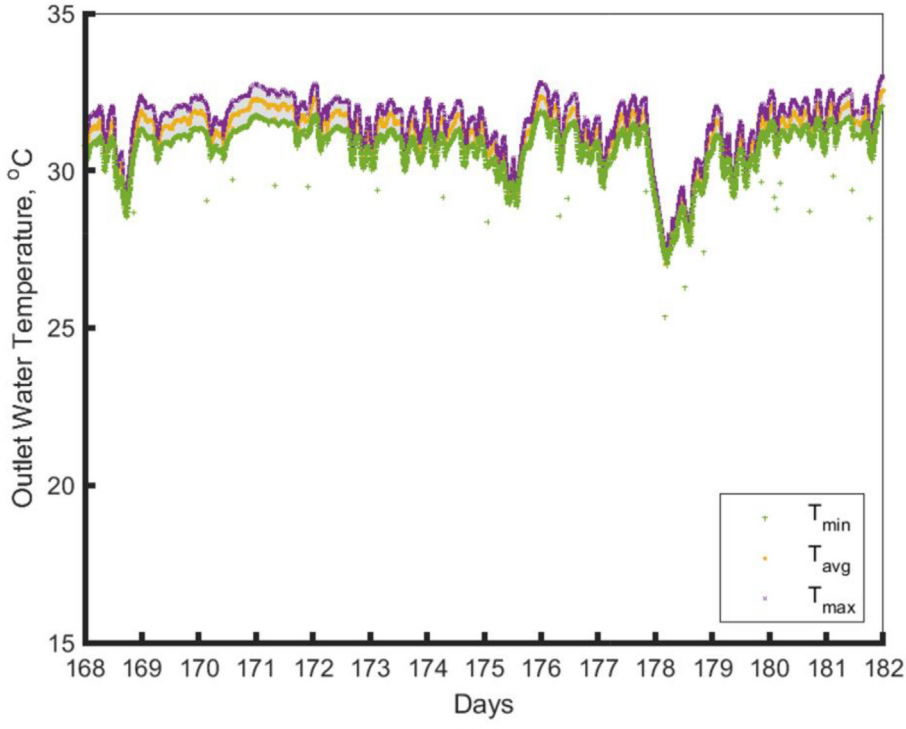

(b)

Fig. 11. The maximum, minimum and average water temperature measured in the separate pipes before the manifold.

similarly as in the beginning of the heating season. The heating supply source was dominated by the BTES subsystem again.

It is worth noting that the heat supplied by the STS subsystem was slightly less in the non-heating season than in the heating season. This somewhat counterintuitive results may be due to the facts that first, the total solar radiation on the tilted collector surface is only 15% higher in the non-heating season than in the heating season. Secondly and more importantly, the inlet temperature of the STS subsystem was relatively high. Moreover, it was higher in the non-heating season (75 °C) than in the heating season (55 °C). The later fact also contributes to a lower heating generation from the STS compared to the designed capacity.

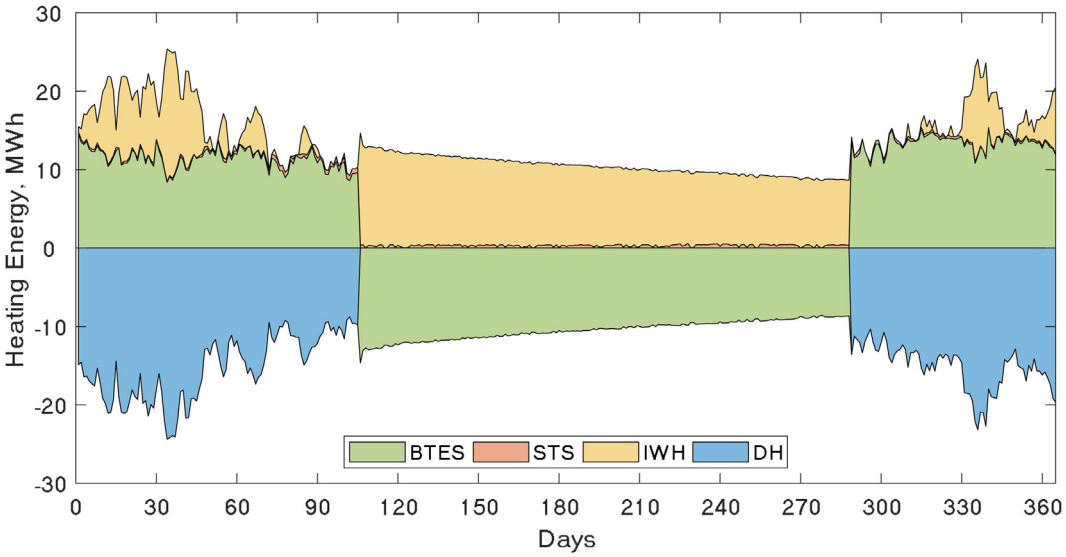

Fig. 12. Daily heat balance for the reference case (overall control, *as is* building insulation level, *standard* weather) in a year.

Fig. 13 presents the *daily average* inlet and outlet water temperature for each subsystem. The color code for each subsystem remain the same as in Fig. 12. The solid lines represent the temperature of the water leaving the subsystem whereas the dotted lines represent the temperature of the water entering the subsystem. It is worth noting that the temperature for the BTES subsystem and the STS subsystem were recorded at the source (primary) side, i.e., the input and output of the borefield and the collector field. The temperature for the IWH and the DH subsystem were recorded in the circulation loop. Therefore, since the IWH subsystem and the DH subsystem are connected in series in the heating season, there are no significant differences between the outlet temperature of the IWH subsystem (the solid yellow line) and the inlet temperature of the DH subsystem (the dotted blue line).

In general, temperature of the STS, IWH and DH subsystems fluctuated greatly whereas the temperatures of the BTES subsystem, especially the outlet temperature, were more stable. In addition, it can be observed that the daily average outlet temperature of the borefield gradually decline throughout the heating season, from around 53 °C to 46 °C. The graph also shows larger distances between the outlet and the inlet temperature of the borefield in the beginning of the heating season (from day 289 to day 318) and slightly reduces through the heating season. Towards the end of the heating season, from around day 30, the distances increase again. The trend in the temperature differences between the inlet and outlet of the borefield also in line with the energy performance of the BTES subsystem as described in Fig. 12.

Fig. 13 shows that the daily average inlet temperature of the DH subsystem was around 45 °C, which seems low compare to the designed heating supply temperature (55 °C). However, it should be stressed that the figure presents the daily average temperature which means that the peaks and valleys are leveled out. Same explanation applies to the STS subsystem as well. More details are provided in Fig. 14 which depicts the hourly inlet and outlet water temperature for each subsystem in a typical winter week (days 3–10 of the year). It shows that the heating supply temperatures were above 50 °C most of the time in the beginning of a day. As for the STS subsystem, the outlet temperature from the solar collectors peaked around midday with a value of 70 °C or even higher.

Last but not least, the outlet temperature of the BTES subsystem only rose for 5 °C throughout the entire non-heating season. Possible explanations are on one hand, the relatively low heating demand to discharge the BTES comparing with the large BTES

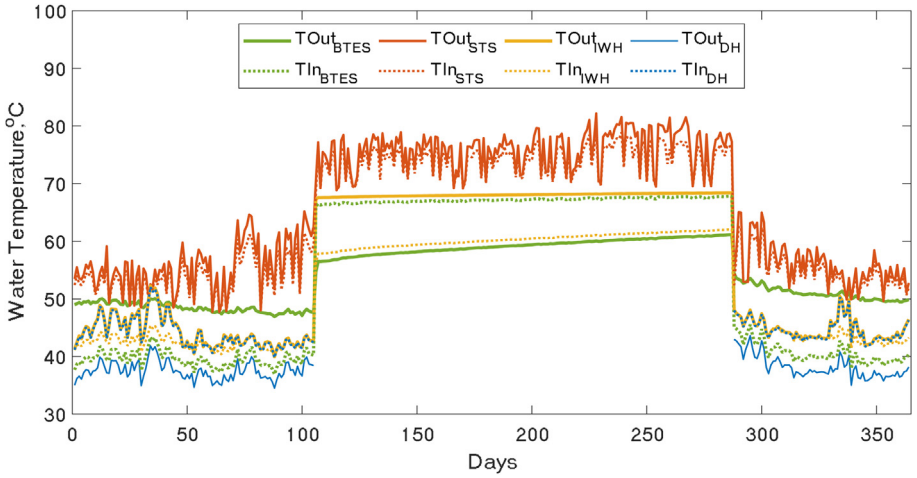

Fig. 13. Daily average inlet and outlet water temperature for each subsystem in a year.

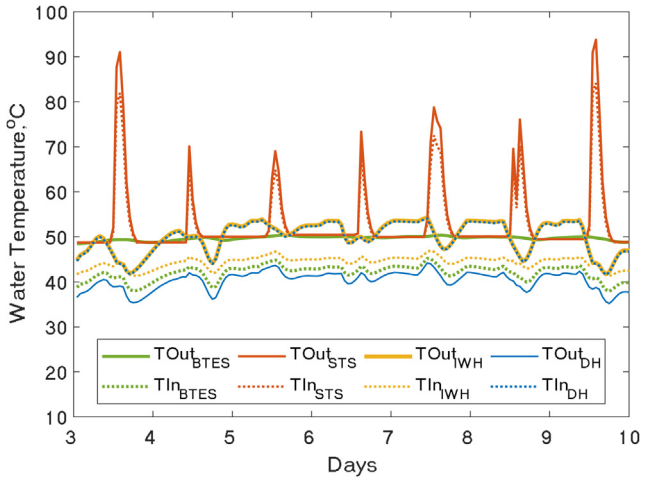

Fig. 14. Hourly inlet and outlet water temperature for each subsystem in a typical winter week (days 3–10 of the year).

capacity; on the other hand, the high operating temperature of the BTES. It's also worth noting that the case study was conducted under the fully charged condition which the core temperature of the BTES reaches 55 °C. The low temperature rise in BTES subsystem during charging also reveals that the BTES capacity is oversized for this case and the performance of the BTES subsystem may not be optimal. However, it should be emphasized that the initial intention of this paper was not to propose an optimized system design but rather verifying, validating and testing the modeling and simulation method for the designed system.

5.2.2. Comparison among the three operation strategies under different scenarios

The results of the reference case show that the supplied heating energy from the BTES subsystem was not well allocated according to the heating demand (refer to Fig. 12). It reveals that the system performance has potential to be improved by investigating the operation strategies of the BTES subsystem. As described in Section 1.4, two other BTES operation strategies are defined: the zonal operation strategy (CM1) and the time-scheduled combined operation strategy (CM2). Fig. 15 depicts the inlet and outlet water temperature of the BTES subsystem operated with the three operation strategies under the six scenarios (Table 5). The subfigures (1) – (6) represent scenario 1 – scenario 6 respectively. Similar to Fig. 13, the *daily average* inlet and outlet water temperatures are shown on the y-axes. However, it should be noted that the x-axes show the days of the heating season instead of the days of the whole year. The day 1 of the heating season is 16th of October (day 289 of the year).

For the *Ref* cases, as shown in the graph, the inlet and outlet temperatures gradually decreased through the heating season, represented by the red lines. It is clearly shown in Fig. 15 (1), (2), (4) and (5) that the differences between the inlet and outlet temperature decreased and reached at the lowest around the day 100 of the heating season (end of January) and rose again for the weather scenario *Standard* and *Extreme*. However, for the *Mild* weather scenario, as shown in Fig. 15 (3) and (6), the temperature differences did not show such trend. This is mainly due to the relatively higher outdoor temperature in the *Mild* weather scenario which resulted in lower heating supply temperatures. Therefore the inlet temperature of the BTES subsystem was lower.

For both CM1 and CM2 cases, the outlet water temperature of the BTES subsystem were lower than the corresponding Ref cases as long as only one zone of the BTES was under operation. The sudden temperature rises indicate the operation mode switches from the zonal control to the overall control. For the CM1 cases, the outlet temperature of the BTES subsystem did not decrease along the heating season as in the *Ref* cases. For the CM2 cases, in the first thirty days, the inlet and outlet temperature were the same as the CM1 cases (around 40 °C for the *As is* scenarios and 45 °C for the *Current regulation* scenarios) since they were in the same operation mode (only one zone was under operation). Then in the CM2 cases, the operation mode switched to the overall control mode and the outlet temperature rose to around 50 °C for the *As is* scenarios and round 52 °C for the *Current regulation* scenarios. It can also be observed from Fig. 15 that a higher outlet temperature in the CM1 and CM2 cases when switching to the overall control mode. A possible explanation is that in the Ref cases, the BTES was discharged at its maximum from the beginning of the heating season though the heating demand was still not too high. This results in a lower outlet temperature in the later days of the heating season for the Ref cases. In the CM1 and CM2 cases, the outlet temperature of the BTES were lower in the beginning and more heating was provided by the backup IWH subsystem to compensate. Then the BTES would be able to provide more heating in the later days of the heating season when the demand is high. This result is in line with the purpose of the zonal strategy and the time-scheduled strategy, i.e., to stabilize the outlet temperature of the BTES throughout the heating season and to better allocate the heating energy of the BTES.

Something unexpected happened with CM1 under scenario 3, refer to the blue lines in Fig. 15 (3), the BTES subsystem switched to the overall control mode after around day 50 of the heating season. This seems too early for a *Mild* weather scenario, moreover the building heating demand is supposed to be the lowest among the three weather scenarios. This happened probably due to a restriction of the BTES model. As described in Table 1, the BTES model cannot provide the average borefield temperature as an output. Therefore, in the simulations, the average borehole wall temperature was chosen as the monitored storage temperature of the BTES. However, the borehole wall temperature shows much larger fluctuation compared to the borefield temperature. It is possible that around day 50, the borehole wall temperature happened to fluctuate under the setpoint which cause an early mode switching. A similar temperature valley can be observed from the solid blue line in Fig. 15 (6) with the case of better building insulation level in the mild climate. In real system operation, the average soil temperature should be used as the control parameter to implement the zonal and time-scheduled operation strategy.

Table 6 lists the total amount of generated/consumed heat of each subsystem in the heating season. Each value is the average number among the six scenarios. It is obvious that in the heating season, BTES performs as the main heat source to supply heating to end users for all the three operation strategies. The amount of heat supplied by the STS subsystem is almost the same among the three operation strategies. The reason is mainly due to the relatively small capacity of the STS subsystem in the initial phase of the living lab. The heat supplied by BTES increases when changing the BTES operation strategies from Ref to CM1 and CM2. Detailed comparison among the three operation strategies are presented in the following texts.

Fig. 16 shows the BTES coverage ratio among the three operation strategies. For the cases with the overall operation strategy (Ref), the BTES subsystem covered 73% to 95% of total heating demand under different scenarios. The BTES coverage ratio decreased to 50% to 83% when the zonal operation strategy (CM1) was applied. The cases with the time-scheduled combined operation strategy (CM2) gave the highest BTES coverage ratio, which ranged from 77% to 96%.

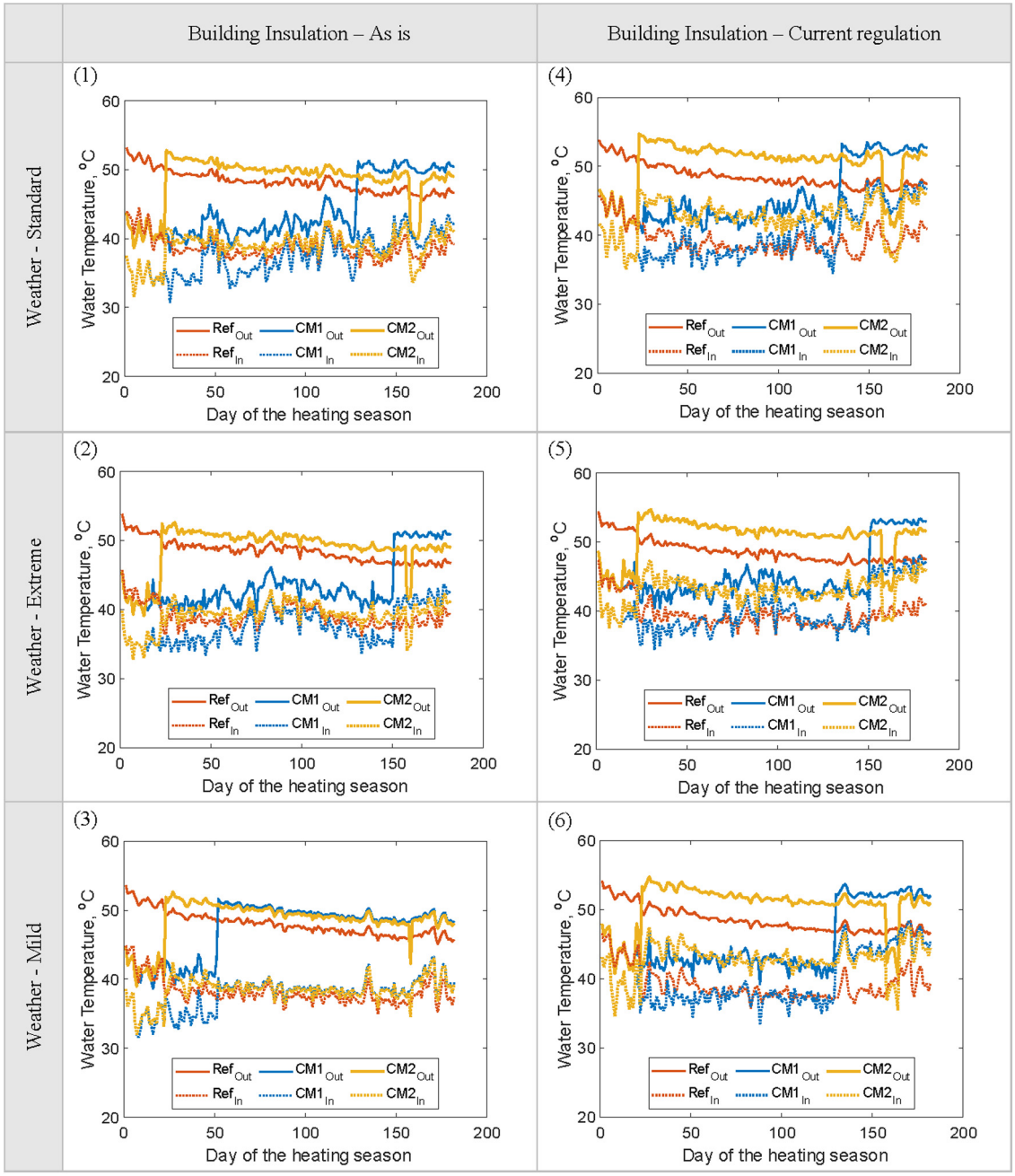

Fig. 15. Comparison on the daily average inlet and outlet temperature for the BTES subsystem in the heating season among different BTES operation strategies at different weather and building insulation scenarios; Ref- overall control, CM1- zonal control, CM2- time-scheduled combined control.

Table 5
Scenario definition.

No.	1	2	3	4	5	6
Building Insulation	As is	As is	As is	Current regulation	Current regulation	Current regulation
Weather	Standard	Extreme	Mild	Standard	Extreme	Mild

As the main purpose of the project was to promote the use of RES, more heating supplied by the BTES and STS subsystem is preferred. In other words, the system with the lowest usage of the backup IWH source would be considered to perform the best. Fig. 17 depicts the comparison among the three BTES operation strategies. Results for different operation strategies are represented by different symbols. The circle symbol o represents the overall operation strategy. The cross symbol × represents the zonal operation strategy. The time-scheduled combined operation strategy is represented by the plus sign + . As shown in Fig. 17(a), the

Table 6
Heat generation (positive value) and consumption (negative value) of each subsystem in the heating season (Unit: GWh).

	Ref	CM1	CM2
STS	0.07	0.08	0.08
BTES	1.95	1.54	2.10
IWH	0.45	0.71	0.27
DH	−2.34	−2.21	−2.31

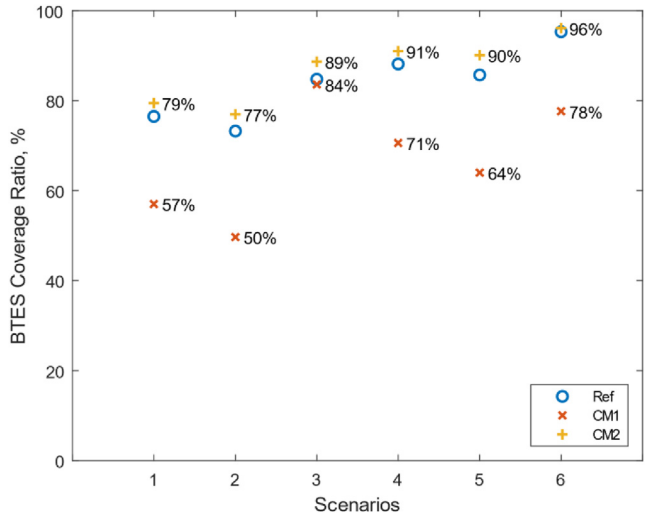

Fig. 16. Comparison on BTES coverage ratio among different BTES operation strategies.

peak heating power ranged from 30 kW to 790 kW for the best cases and from 440 kW to 950 kW for the worst cases. The ranks of the three BTES operation strategies were identical across different scenarios for the peak heating power. The system with the time-scheduled combined operation strategy (CM2) required the lowest peak heating power from the backup IWH source (IWH2) despite the change in building insulation levels and weather conditions. The time-scheduled combined operation strategy benefitted more for buildings renovated to meet the current design standard of energy efficiency for public buildings. The system only needed 30 kW if the buildings were well-insulated and weather was mild. The size of the back-up IWH subsystem is equivalent to a boiler to supply space heating and domestic hot water for a four-bedroom dwelling, which is relatively small for a six building-block site. The three operation strategies rank differently in aggregated heating energy supplied by the backup waste heat source. As shown in Fig. 17 (b), the system with the zonal strategy (CM1) consumed the most from IWH2 heat source throughout the whole heating season among the three operation strategies. The system with the time-scheduled combined operation strategy required the smallest amount of heat from the back-up IWH subsystem.

Overall, adopting the zonal operation strategy brought a small decrease in peak heating power from the back-up IWH subsystem compared to the Ref operation strategy. Considerable improvements happened for scenarios 3, 4 and 5. However, the peak heating power in the "better" scenarios fell into the same range as the Ref method if all scenarios are considered. In addition, the cases of the zonal operation strategy performed the worst in terms of aggregated heating energy supplied by the backup waste heat source in the whole heating season. In contrast, the improvement in both peak heating power and aggregated heating energy were

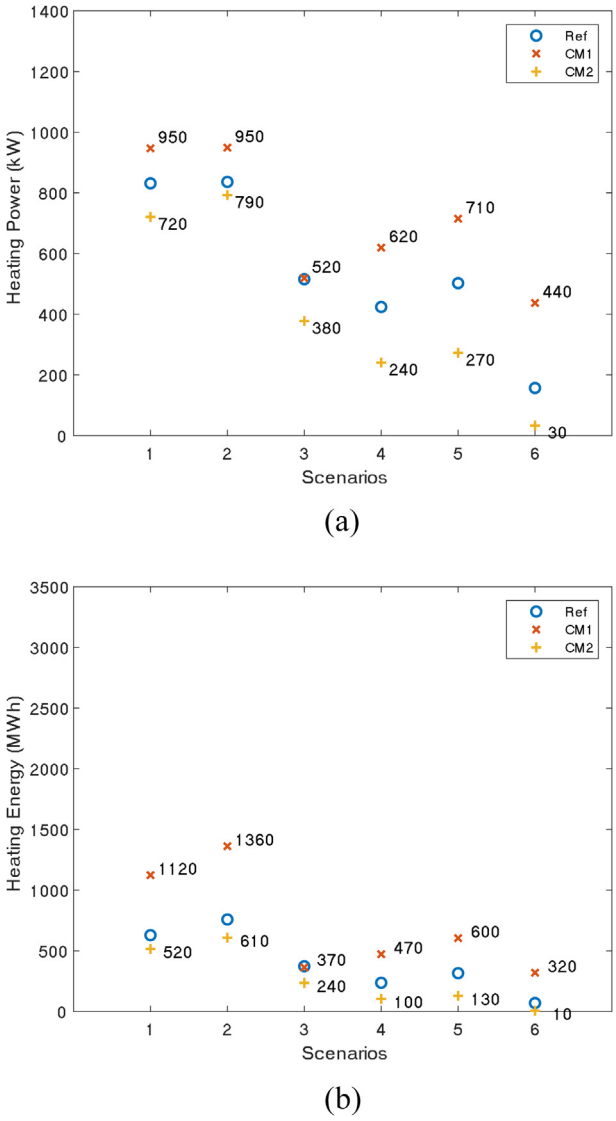

Fig. 17. Comparison on peak heating power (a) and heating energy (b) supplied by IWH2 in the heating season among different BTES operation strategies; Ref- overall control, CM1- zonal control, CM2- time-scheduled combined control.

significant when applying the time-scheduled combined operation strategy. BTES subsystems of the CM2 cases covered at least 10% more than the Ref cases and the CM1 cases. Therefore, the time-scheduled combined operation strategy was more beneficial for the studied system.

6. Conclusion

This research set out to assess the energy performance of different BTES operation strategies for a seasonal solar-industrial waste heat storage in the Chifeng city district heating system.

The research adopted Modelica models from open source libraries to evaluate the system. The validity of the borehole thermal energy storage model was evaluated through an inter-model comparison study and an empirical validation test. The results of the inter-model comparison study show small differences between the Modelica model and the TRNSYS model in injected/extracted heat and outlet water temperature for single borehole cases. The

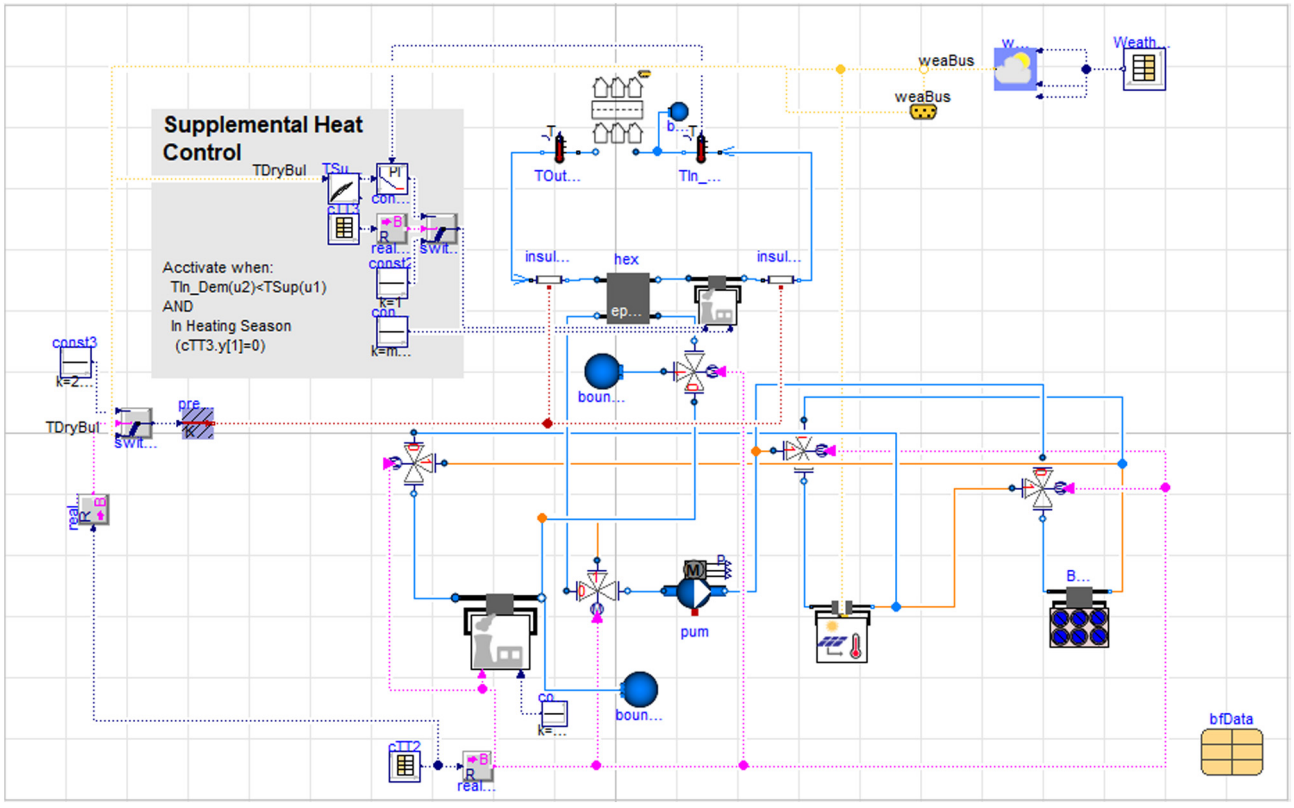

Fig. B1. Layout of the modeled system in Dymola, dashed lines represent control signals, solid lines represent fluid connections.

differences for the borefield cases are slightly larger but still less than 13% for the injected/extracted heat and less than 4 °C for the average hourly outlet water temperature. The result of the empirical validation test further enhances the credibility of the BTES model. It should be noted that the Modelica model is not able to provide the soil temperature in the storage and the heat losses to the air and the surrounding ground. The lack of the two outputs makes it challenging in presenting the energy balance on the BTES. Therefore, it is recommended to use the model if the study focuses on the overall performance of the whole system rather than on the efficiency of the BTES. The Modelica model would require further adaption to further investigate the detailed performance of the BTES.

With the validated model, different BTES operation strategies were investigated. The results show the time-scheduled combined operation strategy is more beneficial for the studied system. The methods used for this system may be applied to evaluating energy performance of other district heating systems with borehole thermal energy storage. The findings of the BTES operation strategy could be of interest to system operators in practice. It is worth noting that the findings of this research are based on predefined weather conditions and occupant schedules. Future research could usefully explore how these uncontrolled factors would influence the system performance.

Declaration of Competing Interest

The authors declare that they have no known competing financial interests or personal relationships that could have appeared to influence the work reported in this paper.

Acknowledgements

This research is part of the seasonal storage for solar and industrial waste heat utilization for urban district heating project funded by the Joint Scientific Thematic Research Programme (JSTP) – Smart Energy in Smart Cities (project No. 467-14-002) and the International S&T Cooperation Program of China (ISTCP) (project No. 2015DFG62410). We gratefully acknowledge the financial support from the Netherlands Organization for Scientific Research (NWO) and Ministry of Science and Technology of the People's Republic of China (MoST). We would also like to thank our industrial partners from Chifeng Heran Energy-saving Science and Technology Co. Ltd. supporting the installation of the living laboratory in Chifeng. Without their efforts and cooperation, we would not have been able to obtain the measurements to conduct the case study.

Appendix A. Design parameters of the investigated system

Table A1
General building properties.

Buildings	Total area (m^2)	Stories	Window-to-wall ratio
Office 1	4230	3	0.34
Dormitory1	2988	4	0.30
Multi-use building	10,390	6	0.26
Laboratory	913	3	0.25
Office 2	495	2	0.17
Dormitory 2	217	1	0.10

Appendix B Layout of the modeled system in Dymola

Fig. B1 presents the layout of the modeled system showing the connections of the sub models in Dymola. The grey box shows model components for controlling the operation of the back-up IWH subsystem (IWH2).

Table A2
Design parameters of the subsystems IWH, BTES and STS.

Parameters	Value	Parameters	Value
Industrial waste heat (IWH)		Distribution network	
Capacity	32.4 GWh/year	Supply temperature	55 °C
Nominal flow rate	47 m^3/h (secondary loop)	Return temperature	45 °C
	300 m^3/h (primary loop)	Circulating flow rate	30 m3/h
Borehole thermal energy storage (BTES)		Solar thermal system (STS)	
Storage type	Single U-tube borehole	Area of collectors	1002 m^2
Storage volume	519,615 m^3	Tilt angle	55°
Storage capacity	2.94 GWh/year	Azimuth angle	8° (0° for south-facing)
Number of boreholes	468	Capacity	0.416 GWh/year
Drilling depth	80 *m*	Buffer tank volume	0.5 m^3
Borehole diameter	150 mm		

Appendix C List of model components for each subsystem

Table C1
List of model components for each subsystem.

Component	Model name	Library
Solar Thermal Subsystem		
Pump	Buildings.Fluid.Movers.FlowControlled_m_flow	Buildings v5.1.0
Tank	IDEAS.Fluid.Storage.StorageTank_OneIntHX	IDEAS v1.0.0
Solar collector	Buildings.Fluid.SolarCollectors.ASHRAE93	Buildings v5.1.0
Heat exchanger	Buildings.Fluid.HeatExchangers.ConstantEffectiveness	Buildings v5.1.0
Solar thermal controller	IDEAS.Controls.ControlHeating.Ctrl_SolarThermal_Simple	IDEAS v1.0.0
Borehole Thermal Energy Storage Subsystem		
Borefield	IDEAS.Fluid.HeatExchangers.GroundHeatExchangers.Borefield.MultipleBoreHolesUTube	IDEAS v1.0.0
Pump	Buildings.Fluid.Movers.FlowControlled_m_flow	Buildings v5.1.0
Heat exchanger	Buildings.Fluid.HeatExchangers.ConstantEffectiveness	Buildings v5.1.0
Industrial Waste Heat Subsystem		
Heat exchanger	Buildings.Fluid.HeatExchangers.ConstantEffectiveness	Buildings v5.1.0
Valve	IDEAS.Fluid.Actuators.Valves.Simplified.ThreeWayValveSwitch	IDEAS v1.0.0
Mass input	Buildings.Fluid.Sources.MassFlowSource_T	Buildings v5.1.0
Valve control	Modelica.Blocks.Interfaces.BooleanInput	Modelica v3.2.2
District subsystem		
Thermal zone	Buildings.ThermalZones.ReducedOrder.RC.OneElement	Buildings v5.1.0
Equivalent air temperature	Buildings.ThermalZones.ReducedOrder.EquivalentAirTemperature.VDI6007WithWindow	Buildings v5.1.0
Infiltration	Modelica.Fluid.Sources.MassFlowSource_T	Modelica v3.2.2
Radiator	Buildings.Fluid.HeatExchangers.Radiators.RadiatorEN442_2	Buildings v5.1.0
Pump	Buildings.Fluid.Movers.FlowControlled_m_flow	Buildings v5.1.0
Weather data reader	Buildings.BoundaryConditions.WeatherData.ReaderTMY3	Buildings v5.1.0

References

[1] National Bureau of Statistics of China, China Statistic Year Book 2015. China Statistic Press, 2015.

[2] National Development and Reform Commission, "The 13th Five-Year Plan on Renewable Energy Development," National Development and Reform Commission (NDRC), 2016.

[3] H. Lund et al., 4th Generation District Heating (4GDH): Integrating smart thermal grids into future sustainable energy systems, Energy 68 (2014) 1–11.

[4] R. Elhashmi, K.P. Hallinan, A.D. Chiasson, Low-energy opportunity for multi-family residences: a review and simulation-based study of a solar borehole thermal energy storage system, Energy 204 (2020) 117870.

[5] A. Dahash, F. Ochs, M. B. Janetti, and W. Streicher, "Advances in seasonal thermal energy storage for solar district heating applications: A critical review on large-scale hot-water tank and pit thermal energy storage systems," Appl. Energy, vol. 239, no. October 2018, pp. 296–315, Apr. 2019.

[6] P. Fitzpatrick, F. D'Ettorre, M. De Rosa, M. Yadack, U. Eicker, D.P. Finn, Influence of electricity prices on energy flexibility of integrated hybrid heat pump and thermal storage systems in a residential building, Energy Build. 223 (2020) 110142.

[7] A. Del Amo, A. Martínez-Gracia, T. Pintanel, A.A. Bayod-Rújula, S. Torné, Analysis and optimization of a heat pump system coupled to an installation of PVT panels and a seasonal storage tank on an educational building, Energy Build. 226 (2020) 110373.

[8] L.T. Terziotti, M.L. Sweet, J.T. McLeskey, Modeling seasonal solar thermal energy storage in a large urban residential building using TRNSYS 16, Energy Build. 45 (2012) 28–31.
[9] D. Olsthoorn, F. Haghighat, P.A. Mirzaei, Integration of storage and renewable energy into district heating systems: A review of modelling and optimization, Sol. Energy 136 (2016) 49–64.
[10] H. Lund et al., The status of 4th generation district heating: Research and results, Energy 164 (2018) 147–159.
[11] B. Welsch, L. Göllner-Völker, D.O. Schulte, K. Bär, I. Sass, L. Schebek, Environmental and economic assessment of borehole thermal energy storage in district heating systems, Appl. Energy 216 (2018) 73–90.
[12] R. McKenna, D. Fehrenbach, E. Merkel, The role of seasonal thermal energy storage in increasing renewable heating shares: a techno-economic analysis for a typical residential district, Energy Build. 187 (2019) 38–49.
[13] M. Reuss, "The use of borehole thermal energy storage (BTES) systems," in Advances in Thermal Energy Storage Systems, Elsevier, 2015, pp. 117–147.
[14] P. D. Thomsen and P. M. Overbye, "Energy storage for district energy systems," in Advanced District Heating and Cooling (DHC) Systems, Elsevier, 2016, pp. 145–166.
[15] G. Alva, Y. Lin, G. Fang, An overview of thermal energy storage systems, Energy 144 (2018) 341–378.
[16] F. Guo, X. Zhu, J. Zhang, X. Yang, Large-scale living laboratory of seasonal borehole thermal energy storage system for urban district heating, Appl. Energy 264 (2020) 114763.
[17] S.C. Johnson et al., Selecting favorable energy storage technologies for nuclear power, in: Storage and Hybridization of Nuclear Energy, Academic Press, 2019, pp. 119–175.
[18] L.F. Cabeza, I. Martorell, L. Miró, A.I. Fernández, C. Barreneche, Introduction to thermal energy storage (TES) systems, in: Advances in Thermal Energy Storage Systems, Elsevier, 2015, pp. 1–28.
[19] K. S. Lee, "Underground Thermal Energy Storage," in Underground Thermal Energy Storage, London: Springer London, 2013, pp. 15–26.
[20] F.M. Rad, A.S. Fung, Solar community heating and cooling system with borehole thermal energy storage – Review of systems, Renew. Sustain. Energy Rev. 60 (2016) 1550–1561.
[21] L. Zhu, S. Chen, Y. Yang, Y. Sun, Transient heat transfer performance of a vertical double U-tube borehole heat exchanger under different operation conditions, Renew. Energy 131 (2019) 494–505.
[22] J. Luo, H. Zhao, J. Jia, W. Xiang, J. Rohn, P. Blum, Study on operation management of borehole heat exchangers for a large-scale hybrid ground source heat pump system in China, Energy 123 (2017) 340–352.
[23] H. Fang, J. Xia, A. Lu, Y. Jiang, An operation strategy for using a ground heat exchanger system for industrial waste heat storage and extraction, Build. Simul. 7 (2) (2014) 197–204.
[24] N. Rapantova, P. Pospisil, J. Koziorek, P. Vojcinak, D. Grycz, Z. Rozehnal, Optimisation of experimental operation of borehole thermal energy storage, Appl. Energy 181 (2016) 464–476.
[25] J.D. Spitler et al., Preliminary intermodel comparison of ground heat exchanger simulation models, in: in Proceedings of the eleventh international conference on thermal energy storage, 2009, pp. 14–17.
[26] S. Lanini, F. Delaleux, X. Py, R. Olivès, D. Nguyen, Improvement of borehole thermal energy storage design based on experimental and modelling results, Energy Build. 77 (2014) 393–400.
[27] G. Ciampi, A. Rosato, S. Sibilio, Thermo-economic sensitivity analysis by dynamic simulations of a small Italian solar district heating system with a seasonal borehole thermal energy storage, Energy 143 (2018) 757–771.
[28] S.K. Shah, L. Aye, B. Rismanchi, Multi-objective optimisation of a seasonal solar thermal energy storage system for space heating in cold climate, Appl. Energy 268 (2020) 115047.
[29] D. Bauer, W. Heidemann, H.-J.-G. Diersch, Transient 3D analysis of borehole heat exchanger modeling, Geothermics 40 (4) (2011) 250–260.
[30] L. Lamarche, S. Kajl, B. Beauchamp, A review of methods to evaluate borehole thermal resistances in geothermal heat-pump systems, Geothermics 39 (2) (2010) 187–200.
[31] G. Teza, A. Galgaro, M. De Carli, Long-term performance of an irregular shaped borehole heat exchanger system: analysis of real pattern and regular grid approximation, Geothermics 43 (2012) 45–56.
[32] B. Bouhacina, R. Saim, H.F. Oztop, Numerical investigation of a novel tube design for the geothermal borehole heat exchanger, Appl. Therm. Eng. 79 (2015) 153–162.
[33] Z. Li, M. Zheng, Development of a numerical model for the simulation of vertical U-tube ground heat exchangers, Appl. Therm. Eng. 29 (5–6) (2009) 920–924.
[34] D. Bauer, W. Heidemann, H. Müller-Steinhagen, H.-J.-J.-G. Diersch, Thermal resistance and capacity models for borehole heat exchangers, Int. J. Energy Res. 35 (4) (2011) 312–320.
[35] S. Whitehead, "Determining temperature distribution: A contribution to the evaluation of the flow of heat in isotropic media," Electrician, pp. 225–226, Aug. 1927.
[36] L.R. Ingersoll, H.J. Plass, Theory of the ground pipe heat source for the heat pump, Heat. Pip. Cond. 20 (1948) 119–122.
[37] H.S. Carslaw, J.C. Jaeger, Conduction of Heat in Solids, 2nd ed., Clarendon Press, Oxford, 1959.
[38] P. Mogensen, Fluid to duct wall heat transfer in duct system heat storages, in Proceedings of International Conference on Subsurface Heat Storage in Theory and Practice, 1983.
[39] J.D. Spitler, M. Bernier, Vertical Borehole Ground Heat Exchanger Design Methods, J.D. Spitler and M, Bernier, 2016.
[40] J. Claesson, S. Javed, An analytical method to calculate borehole fluid temperatures for time-scales from minutes to decades, ASHRAE Trans. 117 (2) (2011) 279–288.
[41] J. Claesson, A. Dunand, Heat extraction from the ground by horizontal pipes - a mathematical analysis, Spangbergs Tryckerier AB, Stockholm, Sweden, 1983.
[42] P. Eskilson, Thermal Analysis of Heat Extraction Boreholes, Lund University, 1987.
[43] C. Yavuzturk, J.D. Spitler, A short time step response factor model for vertical ground loop heat exchangers, ASHRAE Trans. 105 (2) (1999) 475–485.
[44] G. Hellström, Heat Storage in the Ground Duct Ground Heat Storage Model, Manual for Computer Code, University of Lund, Lund, Sweden, 1989.
[45] D. Picard and L. Helsen, "A New Hybrid Model For Borefield Heat Exchangers Performance Evaluation," Proc. 10th Int. Model. Conf., pp. 857–866, 2014.
[46] L. Xu, J.I. Torrens, F. Guo, X. Yang, J.L.M. Hensen, Application of large underground seasonal thermal energy storage in district heating system: A model-based energy performance assessment of a pilot system in Chifeng, China, Appl. Therm. Eng. 137 (2018) 319–328.
[47] E. Fabrizio, V. Monetti, Methodologies and advancements in the calibration of building energy models, Energies 8 (4) (2015) 2548–2574.
[48] I.P.M.V.P. Committee "International Performance Measurement and Verification Protocol Concepts and Options for Determining Energy and Water Savings Volume I", U.S Department of Energy 2002 Oak Ridge, TN, US.
[49] Ministry of Housing and Urban-Rural Development of China, "Design standard for energy efficiency of public buildings," China Architecture Industry Press, Beijing, China, 2015.
[50] China Meteorological Bureau, Climate Information Center, Climate Data Office and Tsinghua University, Department of Building Science and Technology, China Standard Weather Data for Analyzing Building Thermal Conditions. Beijing: China Architecture Industry Press, 2005.